

Lead Optimization of a 4-Aminopyridine Benzamide Scaffold To Identify Potent, Selective, and Orally Bioavailable TYK2 Inhibitors

Jun Liang,^{*,†} Anne van Abbema,^{‡,●} Mercedesz Balazs,[∞] Kathy Barrett,[‡] Leo Berezhkovsky,[§] Wade Blair,^{‡,△} Christine Chang,[‡] Donnie Delarosa,[‡] Jason DeVoss,[∞] Jim Driscoll,^{§,▽} Charles Eigenbrot,[#] Nico Ghilardi,^{||} Paul Gibbons,[†] Jason Halladay,[§] Adam Johnson,[‡] Pawan Bir Kohli,[‡] Yingjie Lai,[†] Yanzhou Liu,[†] Joseph Lyssikatos,[†] Priscilla Mantik,[⊥] Kapil Menghrajani,[§] Jeremy Murray,[#] Ivan Peng,[∞] Amy Sambrone,[⊥] Steven Shia,[#] Young Shin,[§] Jan Smith,[‡] Sue Sohn,^{||} Vickie Tsui,[†] Mark Ultsch,[#] Lawren C. Wu,^{||} Yisong Xiao,[○] Wenqian Yang,[×] Judy Young,[‡] Birong Zhang,[†] Bing-yan Zhu,[†] and Steven Magnuson[†]

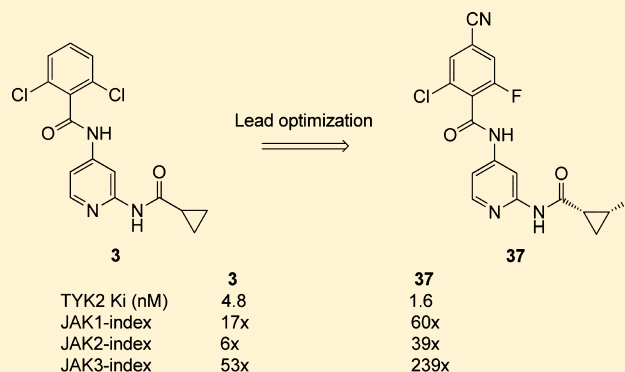
Departments of [†]Discovery Chemistry, [‡]Biochemical and Cellular Pharmacology, [§]Drug Metabolism and Pharmacokinetics, ^{||}Immunology, [⊥]Formulation, [#]Structural Biology, and [∞]Translational Immunology, Genentech, Inc., 1 DNA Way, South San Francisco, California 94080, United States

[×]ChemPartner Co. Ltd., 998 Halei Road, Zhangjiang Hi-Tech Park, Shanghai, 201203, P. R. China

[○]WuXi AppTec Co., Ltd., 288 Fute Zhong Road, Waigaoqiao Free Trade Zone, Shanghai, 200131, P. R. China

Supporting Information

ABSTRACT: Herein we report our lead optimization effort to identify potent, selective, and orally bioavailable TYK2 inhibitors, starting with lead molecule 3. We used structure-based design to discover 2,6-dichloro-4-cyanophenyl and (1*R*,2*R*)-2-fluorocyclopropylamide modifications, each of which exhibited improved TYK2 potency and JAK1 and JAK2 selectivity relative to 3. Further optimization eventually led to compound 37 that showed good TYK2 enzyme and interleukin-12 (IL-12) cell potency, as well as acceptable cellular JAK1 and JAK2 selectivity and excellent oral exposure in mice. When tested in a mouse IL-12 PK/PD model, compound 37 showed statistically significant knockdown of cytokine interferon- γ (IFN γ), suggesting that selective inhibition of TYK2 kinase activity might be sufficient to block the IL-12 pathway *in vivo*.



INTRODUCTION

Psoriasis and inflammatory bowel diseases (IBD), which include Crohn's disease and ulcerative colitis, are both chronic inflammatory disorders of epithelial cells triggered by an overly activated immune system.^{1,2} Psoriasis is a chronic skin disease characterized by red and scaly skin plaques, which is estimated to affect ~2% of the general population.³ In its moderate to severe form where topical application of corticosteroid is no longer effective, psoriasis can present a substantial burden on the well-being of patients.⁴ IBD is a chronic inflammation of epithelial cells lining the gastrointestinal tract and colon that affects approximately 1.4 million patients in United States alone.⁵ Recent approvals of several antitumor necrosis factor (anti-TNF) antibodies represent a major step forward in terms of treatment options for IBD.⁶ However, it is reported that one-third of IBD patients do not respond to anti-TNF therapy. For those who do respond initially, loss of response occurs in 23–46% of patients annually, most often because of development of

antidrug antibodies.⁷ Therefore, significant unmet medical needs still exist for both psoriasis and IBD.

Although clinically distinct, psoriasis and IBD were reported to be associated in some patient populations and show overlapping genetic predispositions, suggesting a shared etiological basis.⁸ Extensive research confirmed that aberrant T cells and their associated extracellular signaling molecules called cytokines play significant roles in the pathogenesis of both diseases.⁹ Of particular importance are T helper type 1 (Th1) and T helper type 17 (Th17) cells. Th1 cells produce cytokine IFN γ , which in turn stimulates innate and T cell-mediated immune response.¹⁰ Overstimulated Th1 cells, however, cause tissue damage and result in chronic inflammation. The more recently discovered Th17 cells, which secrete cytokine IL-17, have been quickly recognized as key players in many autoimmune diseases including psoriasis

Received: February 20, 2013

Published: May 14, 2013

and IBD.¹¹ Th1 and Th17 cell differentiations are driven by IL-12 and IL-23, respectively.¹² Both IL-12 and IL-23 are heterodimeric proteins that share a common subunit designated p40. The receptor for IL-12 consists of two subunits IL-12R β 1 and IL-12R β 2,¹³ whereas the receptor for IL-23 shares the IL-12R β 1 subunit and has a unique subunit called IL-23R.¹⁴ The IL-12 and IL-23 receptors lack intrinsic enzymatic activity. Instead, IL-12R β 1 is known to be constitutively associated with the TYK2 enzyme,¹⁵ while IL-12R β 2 and IL-23R are constitutively associated with the JAK2 enzyme.¹⁶ Both TYK2 and JAK2 belong to the Janus family of tyrosine kinases (JAK) which also includes JAK1¹⁷ and JAK3.¹⁸

In multiple studies with psoriatic patients, significant elevation of IL-12 and IL-23 was observed in lesional skin compared to normal skin.¹⁹ Consistent with this observation, IL-12 and IL-23 expression decreased after psoriatic treatment.²⁰ Similar results were observed in studies in animal models of psoriasis. Transgenic mice that overexpressed the p40 subunit or nontransgenic mice injected with recombinant IL-23 developed inflammatory skin disease, showing comparable phenotype to psoriatic patients.²¹ Inhibition of both IL-12 and IL-23 pathways by anti-p40 antibodies proved to be therapeutically beneficial in both animal models,²² as well as in patients.²³ Ustekinumab, an anti-p40 antibody, was recently approved by the FDA for treating psoriasis.²⁴

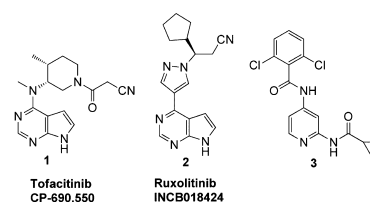
Human genetics studies, especially the recent genome-wide association study, have identified a strong association of IL-23R and IL-12B (encoding the p40 subunit) polymorphisms with IBD.²⁵ Once again, studies with transgenic mice provided further evidence for the importance of the IL-12 and IL-23 pathways in IBD. In well-established T-cell-mediated colitis models, p40 knockout mice were protected from development of intestinal inflammation.²⁶ Finally, the anti-p40 antibody ustekinumab also showed indications of efficacy in certain patients with Crohn's disease.²⁷

We were attracted to the opportunity of blocking the IL-12 and IL-23 signaling pathways in vivo by an orally bioavailable small molecule that inhibits the kinase activity of TYK2 or JAK2 or both. From the outset, however, we believed that inhibition of the JAK2 kinase activity might be highly problematic. JAK2 is associated with signaling of several hematopoietic growth factors, including the erythropoietin (EPO) receptor.²⁸ JAK2 deficiency is embryonically lethal in mice,²⁹ and its inhibition leads to anemia in humans.³⁰ A couple of reports, however, suggested that inhibition of the TYK2 enzyme alone might be tolerated and sufficient to block IL-12 and IL-23 signaling in vivo. TYK2-deficient mice were viable with no gross abnormal phenotype and showed severely impaired signaling and biological response to IL-12 and IL-23 while displaying marked resistance to development of skin inflammation and experimental colitis.³¹ A human patient carrying a TYK2-inactivating mutation was also reported³² and was clinically diagnosed with hyper-IgE syndromes (HIES). Consistent with observations with the TYK2-deficient mice, the human patient's T cells showed almost complete defects in IL-12 and IL-23 signaling, with apparently normal embryogenesis, postnatal growth, and hematopoiesis. Therefore, we were cautiously optimistic that inhibiting the TYK2 kinase activity, while sparing JAK2, might be adequate to block IL-12 and IL-23 signaling in vivo. On the basis of safety considerations, we decided to target a JAK2 selectivity criterion of at least 10-fold in cell-based assays. We have previously shown that the predominant drivers of the IL-12 and EPO pathways are TYK2

and JAK2, respectively.³³ Thus, cellular assays with pSTAT4 and pSTAT5 as proximal readouts of these respective pathways were established to assess TYK2 and JAK2 inhibitions in cells.

Required JAK1 and JAK3 selectivity was more difficult to define at the beginning of our program. JAK1 is essential for signaling of a wide variety of physiologically important cytokines such as IL-6, and its deficiency is perinatally lethal in mice.³⁴ JAK3 expression is mostly restricted to hematopoietic cells and is known to be exclusively associated with the γ common (γ_c) receptor of type I cytokines.³⁵ Inactivating mutation or deletion of JAK3 gene in humans results in severe combined immunodeficiency (SCID).³⁶ Despite the deleterious phenotypes of JAK1- and JAK3-deficient mice and humans, JAK kinase inhibitors, most notably tofacitinib (**1**)³⁷ and ruxolitinib (**2**),³⁸ are reported to be tolerated at efficacious doses during clinical trials at concentrations that only partially inhibit the activity of JAK1 and JAK3. In order to test our hypothesis with a TYK2-selective inhibitor, we decided to tentatively target the JAK1- and JAK3-selectivity criteria of at least 10-fold as measured in cell-based assays as well.

Given the high degree of sequence homology between the JAK family kinases, especially in the ATP binding site where our ATP-competitive inhibitors reside, it was recognized that achieving a high degree of TYK2 selectivity vs other JAKs represented a significant challenge.³⁹ To the best of our knowledge, we are not aware of any published report of selective TYK2 inhibitors except several recent patent applications that appeared after completion of our work.⁴⁰ Toward our goal of discovering potent and selective TYK2 inhibitors, we had identified, through a hit to lead campaign following a high throughput screen, a 4-aminopyridine benzamide lead **3** (Figure 1) with many attractive properties.⁴¹ In biochemical assays, compound **3** showed moderate potency inhibiting the TYK2 enzyme, with modest biochemical



TYK2 $K_i^{a,b}$ (nM)	7.8	0.5	4.8
JAK1 $K_i^{a,b}$ (nM)	0.7	0.2	83.8
JAK2 $K_i^{a,b}$ (nM)	0.7	0.1	27.6
JAK3 $K_i^{a,b}$ (nM)	0.4	3.2	253
IL-12 pSTAT4 ^{c,d} EC ₅₀ (nM)	625	10	380
IL-6 pSTAT3 ^{c,e} EC ₅₀ (nM)	53	24	2000
EPO pSTAT5 ^{c,f} EC ₅₀ (nM)	93	12	1700

Figure 1. Biochemical and cell-based assay data of **1**, **2**, and **3**. ^aBiochemical assays. ^bArithmetic mean of at least four separate runs ($n \geq 4$). On average, the coefficients of variation were less than 0.3 times the mean for biochemical assays. ^cCell-based assays. Arithmetic mean of at least four separate runs ($n \geq 4$). On average, the coefficients of variation were less than 0.5 times the mean for cell-based assays. ^dCell-based assay of TYK2 inhibition. ^eCell-based assay of JAK1 inhibition. ^fCell-based assay of JAK2 inhibition.

selectivity against JAK2 and JAK1 and good selectivity against JAK3.⁴²

In cell-based assays,³³ 3 demonstrated reasonable potency in blocking the IL-12 pathway (IL-12 pSTAT4 EC₅₀ = 380 nM) while displaying less activity in the EPO (JAK2) and IL-6 (JAK1) pathways. Even though the biochemical and cellular potency as well as JAK1 and JAK2 selectivity required improvement, compound 3 represented an important milestone for our program, demonstrating that despite the high sequence homology of ATP-binding pockets between TYK2 and other JAK isoforms, reasonably selective TYK2 inhibitors could be identified. In terms of physicochemical properties, lipophilicity for 3 was somewhat high with measured LogD of 3.4 at pH 7.4.⁴³ We intended to improve potency and selectivity of our analogues without further increase in lipophilicity. In mice, compound 3 exhibited relatively high clearance (65 mL/min/kg) when dosed intravenously (iv 1 mg/kg) and exhibited modest oral exposure (AUC = 2.6 μM·h at po 5 mg/kg) despite excellent cell permeability (MDCK A/B P_{app} = 30 × 10⁻⁶ cm/s) and aqueous solubility (170 μg/mL at pH 7.4). These results suggested that oral exposure in mice for compound 3 might be limited by first-pass metabolism. Since our IL-12 PK/PD experiments would be conducted in mice, it was important to achieve good oral exposure in mice while maintaining low predicted clearance in other species. Herein we describe in detail our lead optimization efforts of compound 3.

RESULTS AND DISCUSSION

To enable design of more potent and selective TYK2 inhibitors, we obtained cocrystal structures of lead molecule 3 with the JH1 domain of the TYK2 and JAK2 enzymes at 2.0 and 2.4 Å resolution, respectively (Figure 2).⁴¹ Significant difference in P-

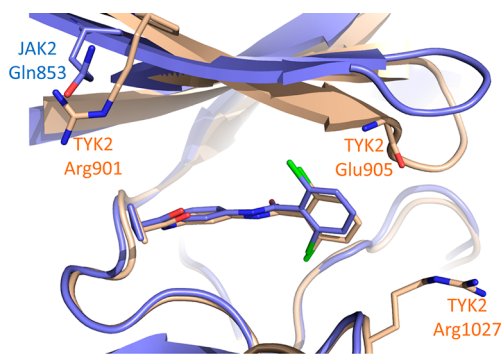


Figure 2. Overlay of the TYK2 and JAK2 crystal structures with compound 3 (TYK2 sandy brown, JAK2 blue), highlighting the different P-loop conformations between the TYK2 and JAK2 enzymes and the residue difference (Arg901 vs Gln853) in the area where cyclopropylamide group was bound. The resolutions of the X-ray structures are 2.0 Å (TYK2) and 2.4 Å (JAK2), respectively.

loop conformation was noted between the two enzymes: in the crystal structure of 3 with the TYK2 enzyme, the P-loop reached down toward the C-terminal lobe, and as a result, the 4-position of the phenyl group is only 3.6 Å from the backbone carbonyl of Glu905 on the tip of the P-loop. On the contrary, the P-loop in the JAK2 enzyme was significantly more “open”. We envisioned that introduction of hydrogen bond (H-bond) donor at the C4-position on phenyl might lead to favorable and specific H-bond interaction with the carbonyl of Glu905 on the TYK2 P-loop, resulting in improved potency and possibly selectivity. It also seemed plausible that substitution at the C4-

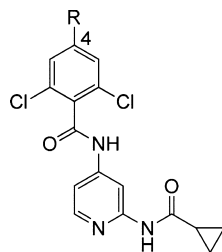
position of the phenyl ring might force the P-loop to move up⁴⁴ so that the C4-substituent could interact with a very polar region containing charged residues such as Arg1027. A second region to potentially capitalize on is where the cyclopropylamide group was bound, for which there is a residue difference between the TYK2 and JAK2 enzymes. In the TYK2 enzyme, this residue is a positively charged arginine (Arg901), while it is a neutral glutamine (Gln853) in JAK2. Even though both residues are on the protein surface and solvent-exposed, we were eager to determine if this difference could be exploited to improve the JAK2 selectivity of our analogues. Initial modeling suggested that substitution at the C2-position of the cyclopropylamide group could provide a vector to access this region.

We started SAR exploration by first focusing on modifications at the C4-position of the 2,6-dichlorophenyl group in compound 3. In addition to the structural rationale outlined above, incubation of compound 3 with human liver microsomes showed formation of two major metabolites resulting from hydrolysis of the cyclopropylamide and oxidation on the 2,6-dichlorophenyl ring, respectively. Meta-site⁴⁵ (Molecular Discovery) analysis predicted that the phenyl C4-position was likely the site of this oxidative metabolic transformation. Therefore, introduction of a functional group, preferably a polar and electron-withdrawing one, might be a viable approach to block such metabolism while simultaneously lowering the associated LogD. Previous structure–activity relationship (SAR) of 4-aminopyridine benzamides from a library of commercially available 2-chlorobenzoic acids had demonstrated that small groups were tolerated at the C4-position of the phenyl ring,⁴¹ so all indications pointed to this being an important region to explore.

Representative analogues from the C4-position SAR and their biological data are listed in Table 1. Enzyme data were used to calculate the biochemical JAK1 and JAK2 indexes, defined as (JAK1 K_i)/(TYK2 K_i) and (JAK2 K_i)/(TYK2 K_i), respectively. For analogues that showed TYK2 enzyme K_i < 5.0 nM, cellular inhibitory activities (EC₅₀) of the IL-12, IL-6, and EPO pathways using pSTAT4, pSTAT3, and pSTAT5 readouts, respectively, were also measured. The cell potency data were then used to calculate the associated cell JAK1 and JAK2 indexes, defined as (IL-6 pSTAT3 EC₅₀)/(IL-12 pSTAT4 EC₅₀) and (EPO pSTAT5 EC₅₀)/(IL-12 pSTAT4 EC₅₀), respectively.

Among compounds with an H-bond donor directly connected to the phenyl ring (compounds 4–7), aniline analogue 4 was found to be the most potent TYK2 inhibitor, with slightly better JAK1 and JAK2 indexes than 3. Phenol 7 was also well-tolerated. When the phenol was converted to a methyl ether (compound 8), a slight loss of potency was observed. Given the potential liabilities of both phenol and aniline, we investigated whether benzyl alcohols or benzylamines, with the H-bond donor removed one atom from the ring, would be suitable replacements. Primary, secondary, tertiary, and propargylic alcohols (compounds 9–12) were introduced at the C4-position. None, however, was as potent as the phenol analogue 7. We also systematically examined primary, secondary, and tertiary benzylamines (compounds 13–16). Likely protonated at physiological pH, the amino groups could not only serve as H-bond donors but also result in significantly lowered lipophilicity. Disappointingly, biochemical data showed that all the benzylamino analogues were less potent than the aniline analogue 4.

Table 1. SAR of Modifications at C4-Position on the Phenyl Ring



Example	R	TYK2 K _i ^a (nM)	JAK1-index ^b (biochemical)	JAK2-index ^c (biochemical)	IL-12 pSTAT4 EC ₅₀ ^d (nM)	JAK1- index ^e (cell)	JAK2- index ^f (cell)
3	H	4.8	17x	6x	380	5x	4x
4	NH ₂	1.0	32x	10x	248	9x	7x
5	NHAc	3.0	37x	14x	393	21x	6x
6	NHSO ₂ Me	13.5	5x	3x			
7	OH	3.1	25x	12x	436	8x	6x
8	OCH ₃	7.8	8x	6x			
9	CH ₂ OH	5.4	13x	7x			
10 (racemic)		7.6	7x	2x			
11		21.8	7x	3x			
12		10.3	6x	5x			
13	CH ₂ NH ₂	4.4	11x	7x	452	7x	9x
14	CH ₂ NHCH ₃	3.3	21x	19x	273	4x	11x
15	CH ₂ N(CH ₃) ₂	60.8	3x	1x			
16		35.1	5x	4x			
17	COCH ₃	7.8	9x	6x			
18	CON(CH ₃) ₂	30.1	12x	3x			
19	CN	1.8	30x	14x	157	8x	11x
20	C≡CH	9.5	11x	6x			
21		3.4	8x	2x	198	3x	3x
22		10.9	10x	5x			

^aBiochemical assays. Arithmetic mean of at least three separate runs ($n \geq 3$). On average, the coefficients of variation were less than 0.3 times the mean for biochemical assays. ^b(JAK1 K_i)/(TYK2 K_i). ^c(JAK2 K_i)/(TYK2 K_i). ^dCell-based assay of TYK2 inhibition. Arithmetic mean of at least three separate runs ($n \geq 3$). On average, the coefficients of variation were less than 0.5 times the mean for cell-based assays. ^e(IL-6 pSTAT3 EC₅₀)/(IL-12 pSTAT4 EC₅₀). ^f(EPO pSTAT5 EC₅₀)/(IL-12 pSTAT4 EC₅₀).

Among other functional groups surveyed at the C4-position, nitrile **19** stood out because of its improved TYK2 K_i (1.8 vs 4.8 nM for **3**) and slightly better biochemical JAK1 and JAK2 indexes. Nitrile isostere-acetylene **20** was approximately 4-fold less potent against TYK2 than nitrile **19**. Heterocycles, in the form of pyrazole and triazole, were also evaluated at the C4-position. Pyrazole **21** was tolerated, although with poor JAK1 and JAK2 selectivities as measured in both biochemical and cellular assays. On the other hand, loss of TYK2 inhibitory

activity was noted for triazole **22**. Additionally, aqueous solubility at pH 7.4 for both **21** and **22** was poor (1 and 2 μg/mL, respectively), possibly because of the addition of one more aromatic ring.⁴⁶ Further exploration of heterocycles at the C4-position was not pursued.

The SAR described above is consistent with the design hypothesis that an H-bond donor such as a primary amino group in compound **4** could have a favorable interaction with the TYK2 enzyme. What we had not predicted, however, was

that compound **19** with a C4-nitrile, typically an H-bond acceptor, would also show improved TYK2 potency. To understand the interaction of nitrile **19** with the TYK2 enzyme, we obtained a cocrystal structure at 2.3 Å resolution (Figure 3).

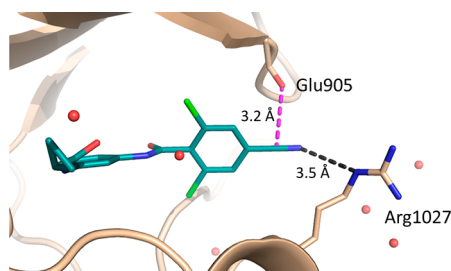


Figure 3. X-ray crystal structure of compound **19** in complex with the TYK2 enzyme. The resolution of the X-ray structure is 2.3 Å.

The distance between the nitrile nitrogen and the Arg1027 NH is 3.5 Å, slightly outside the range of a reasonable H-bond but not excluding the possibility of a long-range electrostatic interaction. Instead, what we noticed was that the P-loop conformation was almost identical to that observed in the TYK2 cocrystal structure with compound **3**. The carbonyl oxygen of Glu905 on the P-loop is 3.2 Å away from the carbon of the nitrile group and likely makes an orthogonal multipolar interaction. This less conventional type of interaction has been observed in the Cambridge small-molecule database (CSD)⁴⁷ and is visually identified by Proasis⁴⁸ (Desert Scientific Software) to be a favorable interaction. We supplemented these empirical observations using *ab initio* calculations of a model system, restraining the distance and angles between the carbonyl and the nitrile carbon atom, and also found this to be an energetically favorable interaction (details in the Experimental Section). One may argue that the potency boost stemmed instead from a nonclassical H-bond between C5-hydrogen of the phenyl and the backbone carbonyl of Glu905, but even though this C5...O distance is 3.4 Å, the angle was not ideal. From an SAR standpoint, the carbon of the C4-nitrile and the nitrogen of the C4-aniline occupied similar space. Both substitutions provided potency gain relative to the C4-hydrogen, with the C4-aniline being approximately 2-fold more potent than the C4-nitrile, supporting our interpretation that the C=O...CN is a favorable polar interaction but is not as strong as an H-bond.

It is remarkable that the P-loop maintained its “closed down” conformation in the cocrystal structures with compounds **3** and **19**, leading us to hypothesize that the TYK2 P-loop is relatively rigid. We believe that the observed TYK2 potency SAR in Table 1 could be rationalized by the “inflexible” P-loop hypothesis. Larger substitutions at the C4-position were tolerated but did not lead to improved potency as designed likely because any favorable interactions to the TYK2 enzyme that such groups facilitated were offset by the energy cost of moving the P-loop. By contrast, aniline **4** could be readily modeled using the TYK2 bound crystal structure of compound **3**:⁴¹ the primary amino group could be accommodated at the 4-position with no movement, and thus no entropic cost, of the P-loop while making a favorable H-bond with the carbonyl of Glu905. This hypothesis could also explain the improved JAK2 index for analogues **4** and **19** as the result of better TYK2 enzyme potency, due to favorable H-bond or orthogonal multipolar interaction with the adjacent P-loop in TYK2. Such

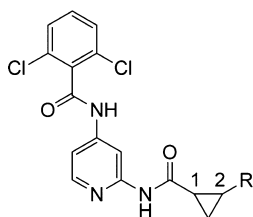
interaction is likely absent with a more “open” JAK2 P-loop. This difference in P-loop conformations between the TYK2 and JAK2 enzymes had been reported previously with other classes of JAK inhibitors.⁴⁹

Despite its better biochemical potency, aniline **4** was less potent in the IL-12 cell assay than nitrile **19** (pSTAT4 EC₅₀ of 248 vs 157 nM). It was encouraging that for both analogues **4** and **19**, the slightly improved biochemical JAK1 and JAK2 indexes translated into slightly better cellular JAK1 and JAK2 indexes than lead molecule **3**. It is also worth pointing out that good cellular JAK1 selectivity was more difficult to achieve than cellular JAK2 selectivity. We suggest this observation is a reflection of the weaker ATP *K_m* for JAK1 compared to JAK2 (55 vs 15 μM).⁵⁰ Compound **19** was profiled against a broad panel of kinases at 180 nM (100-fold in excess of its TYK2 *K_i*) and was found to be reasonably selective. The Gini coefficient of its kinase selectivity was calculated to be 0.65.⁵¹ Among the 187 kinases tested, compound **19** demonstrated >50% inhibition against only six kinases: 80% inhibition against RSK3 and RSK4, 73% against RSK2, 68% against LRRK, and 61% against CDK5 and LCK, respectively.

After determining that a nitrile was the optimal substituent at the C4-position on the 2,6-dichlorophenyl fragment, we then turned our attention to optimization of the cyclopropylamide moiety. As highlighted in Figure 2, there is a residue difference between TYK2 (Arg901) and JAK2 (Gln853) that we hoped to probe through substitution at the C2-position on the cyclopropylamide group. For any given C2-substituent on the cyclopropylamide, *cis*- and *trans*-isomers are possible, with each mixture consisting of a pair of enantiomers. Since the preferred stereochemistry of this substituent could not be predicted with confidence from modeling, we proceeded by preparing and testing both the *cis*- and *trans*-isomers, each as a racemic mixture. If the initial enzyme inhibition data for the racemic mixture were promising, the *cis*- or *trans*-mixture was subject to further purification by chiral HPLC or SFC to give single enantiomers for testing. A general trend quickly emerged from our SAR exploration, where for every C2-substituent evaluated, the racemic *cis*-isomeric mixture was always more potent than the corresponding *trans*-isomeric mixture. Furthermore, when the racemic *cis*-isomers were separated, there was usually a significant difference in the TYK2 potency between the two enantiomers. To illustrate this point, data for four diastereomers of the C2-fluoro analogue (compounds **23–26**) are shown in Table 2. For other C2-substituents, data for only the more active *cis*-enantiomer are included.

When compared to the unsubstituted cyclopropylamide **3**, *cis*-C2-fluoro analogue **23** showed a small but statistically significant improvement in TYK2 enzyme potency (2.5 vs 4.8 nM) and slightly better biochemical JAK1 and JAK2 indexes. The TYK2 enzyme pocket where the cyclopropylamide was bound seemed sensitive to steric bulk. As the size of the C2-substituent increased from F to Cl to CH₃ (compounds **23**, **27**, and **28**), the TYK2 potency gradually decreased. Polar substituents at the C2-position were also examined in hopes of achieving favorable interactions with the polar side chain of Arg901 in the TYK2 enzyme. We expected that polar substituents would also offer an opportunity to reduce the lipophilicity of compound **3**. Contrary to expectations, most of the polar C2-substituents (**29–31**) resulted in reduced TYK2 potency when compared to compound **3**. An exception to this trend was one of the *cis*-enantiomers of carboxylic acid (analogue **32**). It was especially interesting to note that

Table 2. SAR of C2-Substituted Cyclopropylamide



Example ^a	R	Relative stereo	TYK2 K _i ^b (nM)	JAK1-index ^c (biochemical)	JAK2-index ^d (biochemical)
23	F	<i>cis</i>	2.5	47x	19x
24	F	<i>cis</i>	7.1	30x	6x
25	F	<i>trans</i>	11.4	19x	6x
26	F	<i>trans</i>	22.2	3x	6x
27	Cl	<i>cis</i>	5.1	49x	22x
28	CH ₃	<i>cis</i>	8.5	82x	13x
29	CH ₂ OH	<i>cis</i>	14.6	51x	8x
30	CN	<i>cis</i>	9.1	120x	24x
31	CONH ₂	<i>cis</i>	11.1	216x	16x
32	CO ₂ H	<i>cis</i>	3.2	>1000x	390x
33		<i>cis</i>	1.3	62x	30x
34		<i>cis</i>	15.0	15x	4x

^aUnless otherwise indicated, compounds are single enantiomers of unknown absolute configuration. ^bBiochemical assays. Arithmetic mean of at least three separate runs ($n \geq 3$). On average, the coefficients of variation were less than 0.3 times the mean for biochemical assays. ^c(JAK1 K_i)/(TYK2 K_i). ^d(JAK2 K_i)/(TYK2 K_i).

compound **32** showed remarkably high biochemical JAK1 and JAK2 indexes. A single crystal structure of compound **32** was obtained, and its absolute stereochemistry was determined to be *1R,2S* (see Supporting Information). On the basis of the residue difference between the TYK2 and JAK2 enzyme in this area of the binding pocket (Arg901 vs Gln853), we propose that the electrostatic interaction between the positively charged arginine (Arg901) in the TYK2 enzyme and the negatively

charged carboxylate in analogue **32** might partially explain the excellent JAK2 selectivity observed (Figure 4a). This hypothesis, however, does not explain the high degree of JAK1 selectivity for compound **32**. JAK1 and TYK2 share the same residue (arginine) at this position, implying that there might be other significant differences in structure or dynamics between the two enzymes in this area.

As a follow-up to this interesting discovery, we prepared the *cis* enantiomers of the corresponding C2-tetrazole and triazole. The tetrazole **33** was much less selective, although slightly more potent, than the carboxylic acid analogue **32**. Replacement of the acid with triazole (**34**), however, resulted in a 5-fold drop in potency against the TYK2 enzyme. This result is consistent with our hypothesis that the good TYK2 potency observed for acid **32** and tetrazole **33** is partially derived from favorable electrostatic interactions with Arg901. Despite their excellent TYK2 enzyme potencies, acid **32** and tetrazole **33** were both inactive in the TYK2 cell assay (IL-12 pSTAT4 EC₅₀ > 5.0 μM). Both the acid and tetrazole, with calculated pK_a of 3.7 and 4.6, respectively, should be ionized at physiological pH and likely have poor passive cell permeability.

The lack of cell potency for acid **32** and tetrazole **33** underscored the importance of identifying a C2-substituent that was not only potent in biochemical assays but was also cellularly permeable. Fortunately, the C2-fluoro analogue **23** showed excellent cell potency (IL-12 pSTAT4 EC₅₀ = 193 nM). Compound **23** displayed cell JAK1 and JAK2 indexes of 17x and 18x, respectively, meeting our criteria for cellular JAK1 and JAK2 selectivity. Excited by its cell potency and selectivity, we decided to use this particular *cis*-2-fluorocyclopropylamide for future SAR investigation. To define its stereochemistry, we obtained a single crystal X-ray structure of the compound **23** (see Supporting Information) and found that this molecule possessed (*1R,2R*) stereochemistry. We also solved the crystal structure of compound **23** in complex with the TYK2 enzyme at 2.4 Å resolution (Figure 4b). In this cocrystal structure, the fluorine atom is 3.1 Å away from the terminal amino of Arg901. The electronegative fluorine might be slightly favored at the C2-position because of proximity to the positively charged arginine. Since fluorine atoms usually do not act as H-bond acceptors within protein–ligand complexes,⁵² we propose that the favorable dipolar interaction between the C2-fluorine and Arg901 is responsible for the small TYK2 potency improvement of analogue **23**. It was also noteworthy that the distance between the fluorine atom and the

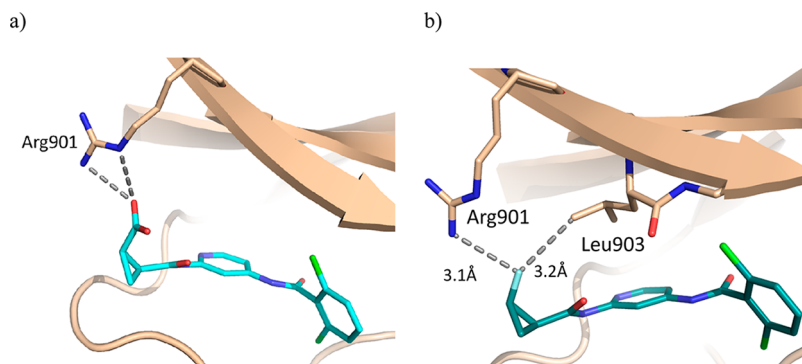
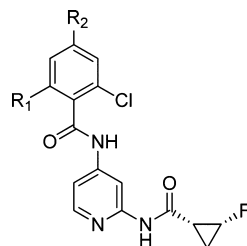


Figure 4. (a) Modeling of acid **32** binding with TYK2 enzyme. The C2-carboxylic acid is proposed to have favorable electrostatic interaction with the positively charged arginine (Arg901) in the TYK2 enzyme. (b) X-ray crystal structure of compound **23** in complex with the TYK2 enzyme. The resolution of the X-ray structure is 2.4 Å.

Table 3. SAR of Combining (1*R*,2*R*)-2-*F*-Cyclopropylamide with Various Benzamides, in Comparison to Ruxolitinib (2)

compd	R ₁	R ₂	TYK2 K _i ^a (nM)	JAK1 index ^b (biochemical)	JAK2 index ^c (biochemical)	JAK3 index ^d (biochemical)	IL-12 pSTAT4 EC ₅₀ ^e (nM)	JAK1 index ^f (cell)	JAK2 index ^g (cell)
35	Cl	CN	1.4	69×	33×	178×	145	16×	20×
36	F	H	1.6	76×	43×	194×	211	24×	22×
37	F	CN	1.6	60×	39×	239×	224	10×	21×
2			0.5	0.4×	0.2×	6×	10	2×	1×

^aBiochemical assays. Arithmetic mean of at least three separate runs ($n \geq 3$). On average, the coefficients of variation were less than 0.3 times the mean for biochemical assays. ^b(JAK1 K_i)/(TYK2 K_i). ^c(JAK2 K_i)/(TYK2 K_i). ^d(JAK3 K_i)/(TYK2 K_i). ^eCell-based assay of TYK2 inhibition. Arithmetic mean of at least three separate runs ($n \geq 3$). On average, the coefficients of variation were less than 0.5 times the mean for cell-based assays. ^f(IL-6 pSTAT3 EC₅₀)/(IL-12 pSTAT4 EC₅₀). ^g(EPO pSTAT5 EC₅₀)/(IL-12 pSTAT4 EC₅₀).

methyl carbon of Leu903 is 3.2 Å, which is approximately the sum of van der Waals radii of both atoms. This compact packing between the C2-fluorine and the methyl group of Leu903 might explain why other groups with larger van der Waals radii, such as chloride or methyl, are not as well-tolerated at this position.

The next logical step in the SAR progression was to combine the (1*R*,2*R*)-2-*F*-cyclopropylamide moiety with our preferred 2,6-dichloro-4-cyanophenyl group (Table 3). We were pleased to find that the potency and selectivity improvement attributed to these two substitutions seemed to be “additive”: analogue 35 was more potent and more selective than either of the predecessor molecules (19 or 23). To better understand the origins of the improved potency and selectivity of analogue 35, we obtained a crystal structure of the inhibitor in complex with the TYK2 enzyme at 2.5 Å resolution (Figure 5). In this crystal

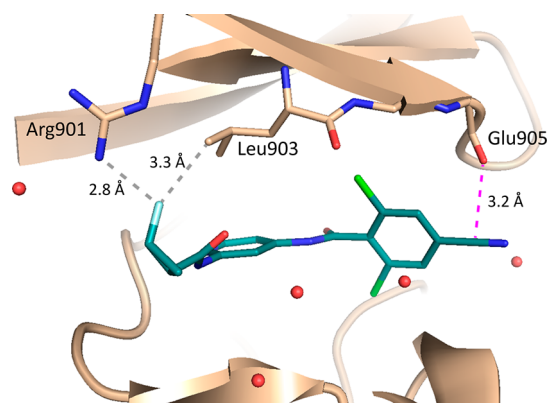


Figure 5. X-ray crystal structure of compound 35 in complex with the TYK2 enzyme. The resolution of the X-ray structure is 2.5 Å.

structure, the fluorine atom is located 2.8 Å away from Arg901, possibly engaged in the same favorable dipolar interaction as observed in the previously described crystal structure of 23 with the TYK2 enzyme. In addition, the carbon atom of the C4-nitrile and the carbonyl oxygen of Glu905 are almost orthogonal to each other with a measured distance of 3.2 Å. This positioning is well within the favorable angle and distance range of an orthogonal multipolar interaction.⁴⁷ We believe that

the SAR observed for compound 35 could be attributed to the presence of both favorable interactions from the fluorine atom as well as the nitrile group with the TYK2 enzyme.

In cell assays, compound 35 was found to be a potent inhibitor of the IL-12 pathway (pSTAT4 EC₅₀ = 145 nM) and displayed excellent cell JAK1 and JAK2 indexes of 16× and 20×, respectively. In order to capitalize on this exciting discovery, we expanded the SAR by preparing analogues with 2-chloro-6-fluorophenyl substitution. In our previous publication,⁴¹ comparable TYK2 potency was observed for 2-chloro-6-fluorophenyl analogue and the corresponding 2,6-dichlorophenyl analogue. We reasoned that replacement of chlorine with fluorine could lower the lipophilicity of our molecules. When the 2-chloro-6-fluorophenyl analogue 36 was prepared and tested in biochemical assays, we were encouraged that it was slightly more active and more selective than analogue 23. Therefore, compound 37, with a C4-nitrile on the phenyl ring, was synthesized. Compound 37 was equipotent to 36, with comparable JAK1 and JAK2 indexes. In cell-based assays, compound 37 showed IL-12 pSTAT4 EC₅₀ of 224 nM, with its cell JAK1 and JAK2 indexes meeting our selectivity criteria. Furthermore, we tested compound 37 in both human peripheral blood mononuclear cells (PBMC) and human whole blood, stimulated with IL-12 in combination with IL-18 and using downstream IFN γ production as a readout.³³ In the PBMC assay, compound 37 showed an EC₅₀ of 168 nM, comparable to its IL-12 pSTAT4 EC₅₀ of 224 nM. In human whole blood, an EC₅₀ of 737 nM was obtained for compound 37.⁵³ Compounds 35, 36, and 37 were also profiled against a broad panel of kinases at concentrations 100 times their corresponding TYK2 K_i values, resulting in Gini coefficients of 0.68, 0.59, and 0.61, respectively. The kinases against which the three analogues showed >50% inhibition were identical to those identified for compound 19.

The physicochemical and in vitro ADME properties of key analogues described in this work are summarized in Table 4, along with data of the initial lead 3 for comparison. Compound 19, which incorporated the 4-nitrile on 2,6-dichlorophenyl ring, was slightly less ligand efficient than 3 (LE of 0.49 vs 0.51), but it was also slightly less lipophilic (LogD of 3.2 vs 3.4). As a result, the calculated lipophilic ligand efficiency (LLE) was higher for 19 than for 3 (5.5 vs 4.9). It was interesting that

Table 4. Physicochemical and in Vitro DMPK Properties of Key Analogues

compd	physicochemical properties					in vitro DMPK properties		
	LE ^a	LLE ^b	log D ^c	tPSA	aqueous solubility (μg/mL) ^d	MDCK A–B P _{app} ^e (×10 ⁻⁶ cm/s)	(ratio (B–A)/(A–B))	plasma protein binding in human, rat, mouse (%)
3	0.51	4.9	3.4	71	170	30	(0.4)	95.1, 95.9, 95.6
19	0.49	5.5	3.2	94	64	15	(1.0)	97.8, 94.1, 96.8
23	0.50	5.7	2.9	71	126	20	(0.8)	97.5, 95.2, 98.2
35	0.48	6.0	2.8	94	74	12	(1.5)	93.2, 91.8, 98.3
36	0.51	ND	ND	71	28	30	(0.4)	93.4, 87.8, 96.4
37	0.47	6.3	2.5	94	53	11	(1.5)	86.6, 91.0, 95.0

^aLigand efficiency = $(-1.4 \log K_i)/(n \text{ heavy atoms})$. ^bLigand–lipophilicity efficiency = $(-\log K_i) - \text{cLogP}$. ^cMeasured log of distribution coefficient between octanol and aqueous pH 7.4 buffer. ^dAqueous solubility was determined in pH 7.4 PBS buffer. ^eApparent permeability in MDCK Transwell culture. A–B: apical-to-basolateral. Ratio is determined by the apparent permeability of B–A basolateral-to-apical divided by A–B apical-to-basolateral.

Table 5. In Vitro Metabolic Stability and in Vivo PK Parameters of Key Analogues

compd	in vitro metabolic stability, LM ^a (mL/min/kg)			in vivo PK									
	human	rat	mouse	rat ^b				mouse ^b				high dose mouse ^c	
				Cl _p (mL/min/kg)	t _{1/2} (h)	V _d (L/kg)	F (%)	Cl _p (mL/min/kg)	t _{1/2} (h)	V _d (L/kg)	F (%)	AUC (μM·h)	C _{max} (μM)
3	7	16	64	21	1.2	1.1	100	65	0.3	0.6	73		
19	8	12	38	3.1	4.2	0.8	86	13	1.0	0.9	100	818	119
23	11	21	55	15	1.8	1.0	100					50	47
35	11	10	36	4.6	4.1	1.0	100					1090	143
36	4	20	64	39	0.5	1.2	100						
37	8	11	34	1.0	40	2.3	70					917	108

^aHepatic clearance predicted from liver microsome stability. ^bMale Sprague rats or CD-1 mice were dosed with each compound iv 1 mg/kg and po 5 mg/kg as a solution in 60% PEG. ^cCD-1 mice were dosed po 100 mg/kg as a MCT suspension.

analogue **23**, with the (1*R*,2*R*)-2-*F*-cyclopropylamide, had an experimental LogD that was 0.5 units lower than that of **3** (2.9 vs 3.4). It has been reported that fluorine substitutions on alkanes, especially in the presence of adjacent oxygen atom, usually result in lowered lipophilicity.^{52a} Through the combination of improved potency and lower LogD, compound **23** has higher LLE than **3** (5.7 vs 4.9). The same trends were observed when the (1*R*,2*R*)-2-*F*-cyclopropylamide and 4-nitrile phenyl group were combined to give compound **35** (LLE = 6.0). Replacement of one of the chlorines on the phenyl ring present in **35** with fluorine yielded compound **37**, which showed an experimental LogD of 2.5, a drop of 0.3 units. Consequently, compound **37** had the highest LLE (6.3) of all analogues in this scaffold. Aqueous solubility of these analogues at pH 7.4 was decent. The cell permeability, as measured in MDCK cells, was high. The plasma protein binding (PPB) of these compounds was examined in human, rat, and mouse. Most of them are highly plasma protein bound. Consistent with its lower lipophilicity, compound **37** showed the lowest plasma protein binding in all three species. It is also interesting to note that for **37**, its plasma protein binding in mouse is considerably higher than in human.

The in vitro metabolic stability and in vivo pharmacokinetic (PK) data of the key inhibitors are summarized in Table 5. Analogue **19** contained the 4-nitrile functionality on the phenyl group, and this substitution was designed to block oxidative metabolism that was observed for compound **3**. No significant difference in human liver microsomal stability, however, was observed between analogues **19** and **3**. Incubation of compound **19** with human liver microsomes showed only a small amount (<2%) of the corresponding cyclopropylamide

hydrolysis product, and no metabolites related to oxidation on the phenyl ring were detected. Comparison of in vivo metabolic stability in mouse and rat between compounds **3** and **19** reveals that addition of C4-nitrile on the phenyl ring clearly had significant impact, as clearance was reduced from 21 to 3.1 mL/min/kg in rat and from 65 to 13 mL/min/kg in mouse, respectively. When compound **19** was dosed orally in mouse at 100 mg/kg, excellent oral exposure (AUC = 818 μM·h) was observed.

For analogue **23**, we were initially concerned that fluorine substitution on the cyclopropylamide would reduce metabolic stability. Cyclopropylamide hydrolysis was one of the major metabolic pathways observed for compound **3**, and the strongly electron-withdrawing fluorine in compound **23** could conceivably, through its inductive effect, render the cyclopropylamide carbonyl even more susceptible to nucleophilic attack. The liver microsomes stability of compound **23** was comparable to **3** in all three species. To confirm these stability trends, we evaluated the clearance of analogue **23** in vivo and obtained a clearance value of 15 mL/min/kg in rat, similar to that of **3** (21 mL/min/kg). When compound **23** was dosed orally at 100 mg/kg in mouse, however, modest exposure (AUC = 50 μM·h) was observed.

When the (1*R*,2*R*)-2-*F*-cyclopropylamide fragment was combined with the 4-cyano-substituted phenyl groups (compound **35** and **37**), attractive PK profiles were obtained. For compound **35** with the 2,6-dichloro-4-cyanophenyl group, the in vitro metabolic stability in rat and mouse was comparable to that of **19**. In vivo, a clearance value of 4.6 mL/min/kg was observed in rat. In a high dose mouse PK experiment with compound **35**, excellent oral exposure (AUC = 1090 μM·h)

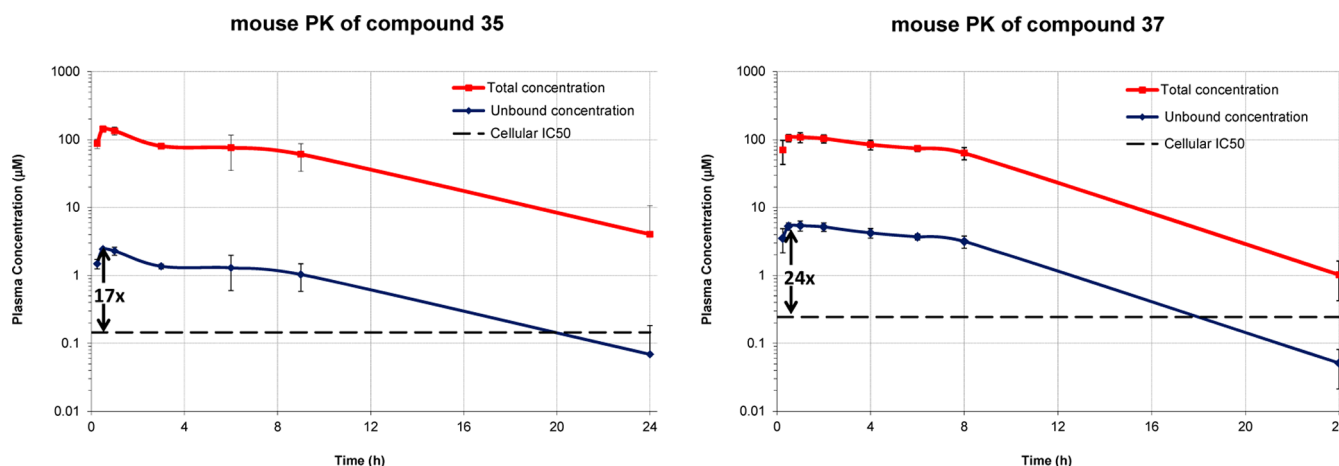


Figure 6. High dose (po 100 mg/kg) mouse PK of compound 35 and 37. Three CD-1 mice were dosed orally with 35 or 37 at 100 mg/kg as a MCT suspension. At different time intervals, a blood sample was taken from each animal and plasma concentration was determined. Reported values were the average of three animals. The unbound concentration was calculated by multiplying the plasma concentration with the corresponding unbound fraction in mouse.

was observed, with maximal total concentration (C_{max}) reaching 149 μM . However, 2-chloro-6-fluoro analogue 36, lacking a 4-nitrile on its phenyl group, showed a relatively high clearance (39 mL/min/kg) in rat. When nitrile was introduced at the C4-position of the phenyl group, resulting in analogue 37, in vitro metabolic stability was comparable to that of compounds 19 and 35. Once again, low clearance (1.0 mL/min/kg) was observed in rat for compound 37, with excellent oral exposure achieved in mouse.

It was gratifying to see that the changes introduced into the lead molecule 3, leading to optimized compounds 35 and 37, improve not only potency and selectivity but also clearance in rat and oral exposure in mouse. With these compounds in hand, we proceeded to in vivo PK/PD studies. While compound 35 was more potent in the IL-12 pSTAT4 assay than 37, it also had higher plasma protein binding in mouse (98.3% vs 95.0%). As a result, unbound drug level relative to its cell EC_{50} for analogue 37 was slightly higher than that for 35 (24x vs 17x) (Figure 6). On the basis of these calculations, compound 37 was selected for in vivo PK/PD study.

To determine if a TYK2-selective inhibitor could inhibit the IL-12 pathway in vivo, a mouse PK/PD model was developed. Administration of recombinant mouse IL-12 in combination with mouse IL-18 resulted in a time- and dose-dependent increase in systemic IFN γ production (data not shown). After optimization of the time and dose required for induction, compound 37 was tested for its ability to inhibit IFN γ production in this model. Anti-p40 antibody, which neutralizes the IL-12 cytokine, was used as a positive control and resulted in near complete (94%) inhibition of IFN γ production (Figure 7a). Thirty minutes prior to cytokine stimulation, ascending doses of 37 were administered orally via gavage (see Supporting Information for the time course of mouse IL-12 PK/PD experiment). Three hours after cytokine stimulation, systemic levels of IFN γ were measured by cytokine ELISA, and total plasma concentration of compound 37 was also determined for this time point. Statistically significant inhibition of the IL-12 pathway was observed for doses of ≥ 10 mg/kg (Figure 7a), with maximal PD response at the 70 mg/kg dose. The lowest dose of 3 mg/kg, however, failed to produce a meaningful pharmacological effect. The 100 mg/kg dose did not give significantly higher unbound drug levels than the 70 mg/kg

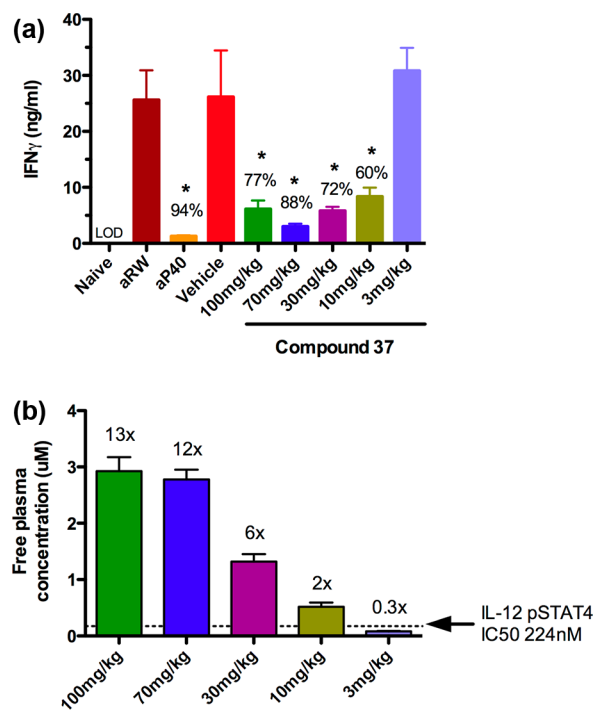
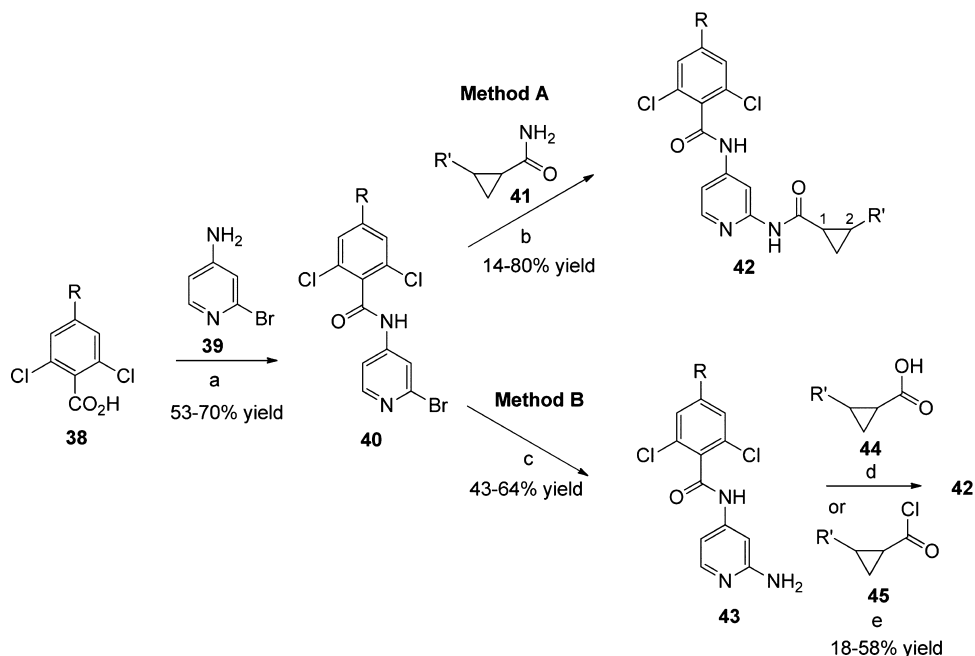


Figure 7. (a) Mouse IL-12 PD response with different doses of compound 37, showing inhibition of IFN γ production by compound 37. Values shown are the average of eight animals at each dose ($n = 8$). Anti-p40 antibody (aP40), which neutralizes IL-12, was used as a positive control. Anti-ragweed antibody (aRW) was used as a negative control. An asterisk denotes $p < 0.05$ compared to control. MCT was used as the vehicle for oral dosing of compound 37. (b) Measured unbound concentration of compound 37 at 3.5 h after oral dosing: plot of the unbound concentration of compound 37 at the 3.5 h time point for different doses. Values shown are the average of eight animals at each dose ($n = 8$). The ratio of unbound concentration of 37 over its IL-12 pSTAT4 EC_{50} was also calculated for all doses.

dose (Figure 7b), and thus, the PD response was comparable. Overall, the PK/PD relationship suggested that a significant attenuation of cytokine IFN γ production could be achieved at doses of 100, 70, 30, and 10 mg/kg when unbound drug

Scheme 1. Preparation of 2-Cyclopropylamides–Pyridyl-4-benzamides^a

^aReagents and conditions: (a) thionyl chloride, toluene, 100 °C; then NaH, DMF, 0 °C; (b) Pd₂(dba)₃, XantPhos, Cs₂CO₃, 1,4-dioxane, 130 °C, microwave; (c) Pd₂(dba)₃, DavePhos, LHMDS, 1,4-dioxane, 100 °C; then 1 N HCl; (d) HATU, DIPEA, DMF, 70 °C; (e) NEt₃, dichloromethane, 0 °C.

concentration is ≥ 2 -fold of the corresponding IL-12 pSTAT4 EC₅₀ value.

CHEMISTRY

Preparation of compounds reported in this work is summarized in Scheme 1, utilizing chemistry similar to what was reported in our previous publication.⁴¹ The syntheses of various benzoic acids are described in the Supporting Information. Briefly, a 2,6-dichlorobenzoic acid **38** was converted to its corresponding acid chloride, which was coupled with 2-bromo-4-aminopyridine **39** to give amide **40**. With 2-bromopyridine **40** in hand, we developed two methods to prepare cyclopropylamide **42** (methods A and B in Scheme 1). A palladium-catalyzed Buchwald coupling reaction of bromide **40** with primary amide **41** (method A) could be carried out smoothly to give cyclopropylamide **42**. Alternatively, the 2-bromopyridine **40** could be first transformed to 2-aminopyridine **43**. Standard amide coupling reactions of 2-aminopyridine **43** with a cyclopropylcarboxylic acid **44**, or an acid chloride **45**, also led to cyclopropylamide **42**.

CONCLUSION

Starting with lead molecule **3**, we carried out comprehensive and systematic SAR investigation of the 2,6-dichlorophenyl and cyclopropylamide moieties, aided by structure-based design. Optimization of the benzamide portion of **3** led to identification of the 2,6-dichloro-4-cyanophenyl group, which showed improved TYK2 potency as well as JAK1 and JAK2 selectivity. This illustrates that selectivity can be obtained not only by directly targeting residue differences but also by utilizing the overall difference in P-loop conformation or flexibility. Furthermore, incorporation of the C4-nitrile substituent reduced clearance in vivo, likely as a result of blocking oxidative metabolism on the phenyl group. Sub-

sequent exploration of various C2-substituent on the cyclopropylamide present in **3** led to identification of the (1*R*,2*R*)-2-fluorocyclopropylamide moiety that further improved TYK2 potency and JAK1 and JAK2 indexes, without compromising metabolic stability. When the two separately optimized moieties were combined, the resulting compound **35** and the closely related analogue **37** displayed excellent cell potency and selectivity profiles. Both analogues also exhibited good oral exposures when dosed in mouse. Accordingly, compound **37** was selected for a mouse PK/PD experiment because of it having the best ratio of unbound drug level in mouse over its cell IL-12 pSTAT4 EC₅₀. Significant suppression of IFN γ production was achieved when compound **37** was dosed at greater than 3 mg/kg in a mouse IL-12 PK/PD model. This result supports our hypothesis that inhibition of the TYK2 kinase alone could lead to blocking of the IL-12 signaling pathway in vivo.

EXPERIMENTAL SECTION

General. Unless otherwise indicated, all reagents and solvents were purchased from commercial sources and used without further purification. Moisture or oxygen sensitive reactions were conducted under an atmosphere nitrogen gas. Unless otherwise stated, ¹H spectra were recorded at room temperature using Varian Unity Inova Bruker AVANCE III UltraShield-Plus Digital NMR spectrometer at indicated frequencies. Chemical shifts are expressed in ppm relative to an internal standard: tetramethylsilane (=0.00 ppm). The following abbreviations are used: br = broad signal, s = singlet, d = doublet, dd = doublet of doublets, t = triplet, q = quartet, m = multiplet. Purification by silica gel chromatography was carried out using a CombiFlash by Teledyne ISCO system with prepacked cartridges. Purification by reverse phase high performance liquid chromatography (HPLC) was also used, and the conditions were described as indicated. Racemic mixtures of final compounds were separated into individual enantiomers by chiral supercritical fluid chromatography (SFC) under the indicated conditions. All final compounds were purified to

>95% chemical purity, as assessed by HPLC (column, Agilent SD-C18, 2.1 mm × 30 mm, 1.8 μm; mobile phases, water with 0.5% TFA, CH₃CN with 0.5% TFA; flow rate of 0.4 mL/min; run time of 8.5 min; oven temperature of 40 °C; UV detection at 254 and 210 nm. In cases where enantiomers or diastereomers were separated by chiral stationary phase HPLC or chiral SFC, the final products were >98% ee or de.

2,6-Dichloro-4-cyano-*N*-(2-(cyclopropanecarboxamido)pyridin-4-yl)benzamide (19). *Step 1.* A solution of 2,6-dichloro-4-cyanobenzoic acid (1.15 g, 5.32 mmol) in thionyl chloride (5.0 mL) was heated to reflux under nitrogen overnight. The next day, the mixture was concentrated via rotavap to give the desired acid chloride as a white solid, which was used in the next step without further purification.

To a solution of 2-bromo-4-aminopyridine (0.912 g, 5.32 mmol) in anhydrous DMF (5.0 mL) at 0 °C was carefully added NaH (0.424 g, 10.6 mmol, 60% dispersion in mineral oil). Ice bath was removed, and the suspension was warmed to room temperature and stirred for 30 min before being cooled to 0 °C again. To this reaction mixture was slowly added a solution of the above acid chloride dissolved in anhydrous DMF (4.0 mL). Ice bath was removed, and the mixture was warmed to room temperature and stirred for 1 h under nitrogen. Ice-water (20 mL) was added, and the reaction mixture was extracted with ethyl acetate (3 × 50 mL). Combined organics were dried over Na₂SO₄, concentrated via rotavap, and purified by flash column chromatography on silica gel (EtOAc/petroleum ether = 1:10) to afford *N*-(2-bromopyridin-4-yl)-2,6-dichloro-4-cyanobenzamide as a white solid (1.18 g, 59% yield). LCMS (ESI) *m/z*: 369.9 [M + H]⁺.

Step 2. A 10 mL microwave tube equipped with a magnetic stirring bar was charged with *N*-(2-bromopyridin-4-yl)-2,6-dichloro-4-cyanobenzamide (74 mg, 0.20 mmol), followed by cyclopropanecarboxamide (34 mg, 0.40 mmol), Pd₂(dba)₃ (18 mg, 0.020 mmol), XantPhos (23 mg, 0.040 mmol), Cs₂CO₃ (131 mg, 0.40 mmol), and 1,4-dioxane (1.2 mL). The tube was flushed with nitrogen for 5 min before being sealed and heated at 140 °C for 1 h in a microwave reactor. The tube was cooled to room temperature, and the reaction mixture was filtered through Celite. The filter cake was washed with additional EtOAc (2 × 5 mL). Combined filtrate was evaporated to dryness and purified by preparative HPLC (Gilson GX 281; column, Shim-pack PRC-ODS 250 mm × 20 mm 15 μm; mobile phase CH₃CN/10 mM NH₄HCO₃; flow rate of 30 mL/min; run time of 17 min) to afford the desired product (30 mg, 40% yield). ¹H NMR (500 MHz, DMSO-*d*₆): δ 11.28 (s, 1H), 10.79 (s, 1H), 8.36–8.24 (m, 4H), 7.47 (m, 1H), 2.00 (m, 1H), 0.81–0.79 (m, 4H). LCMS (ESI) *m/z*: 375.1 [M + H]⁺.

2,6-Dichloro-*N*-(2-((1*R*,2*R*)-2-fluorocyclopropanecarboxamido)pyridin-4-yl)benzamide (23) and 2,6-Dichloro-*N*-(2-((1*S*,2*S*)-2-fluorocyclopropanecarboxamido)pyridin-4-yl)benzamide (24). To a 25 mL round-bottom flask was added *N*-(2-aminopyridin-4-yl)-2,6-dichlorobenzamide (60 mg, 0.213 mmol), followed by anhydrous DMF (2.0 mL), *cis*-2-fluorocyclopropanecarboxylic acid⁵⁴ (111 mg, 1.06 mmol), DIPEA (137 mg, 1.06 mmol), and HATU (404 mg, 1.06 mmol). The reaction mixture was heated at 60 °C under nitrogen for 12 h when monitoring the reaction by LCMS showed complete conversion. The reaction mixture was cooled to room temperature, diluted with saturated NH₄Cl solution (20 mL), and then extracted with EtOAc (3 × 20 mL). The combined organics were dried over Na₂SO₄, filtered, and concentrated via rotavap. The crude product was purified by chiral SFC (Chiralpak IC, 35% IPA + 0.1% NEt₃, 5 min) to give two desired products as the following:

23: second eluting peak, 21 mg (27% yield), >99% ee (retention time 0.87 min, Chiralpak IC, 35% IPA + 0.1% NEt₃, 5 min). ¹H NMR (400 MHz, DMSO-*d*₆): δ 11.15 (s, 1H), 10.77 (s, 1H), 8.39 (s, 1H), 8.24 (d, *J* = 5.6 Hz, 1H), 7.62–7.55 (m, 2H), 7.55–7.43 (m, 2H), 4.91 (dddd, *J* = 66.3, 6.3, 6.2, 3.6 Hz, 1H), 2.21 (dddd, *J* = 9.0, 6.8, 6.3, 5.9 Hz, 1H), 1.65 (dddd, *J* = 23.4, 6.8, 6.7, 3.6 Hz, 1H), 1.16 (dddd, *J* = 12.4, 9.0, 6.8, 6.3 Hz, 1H). LCMS (ESI) *m/z*: 368.0 [M + H]⁺.

24: first eluting peak, 22 mg (28% yield), >99% ee (retention time 0.61 min, Chiralpak IC, 35% IPA + 0.1% NEt₃, 5 min). ¹H NMR and LCMS match 23.

2,6-Dichloro-*N*-(2-(*trans*-2-fluorocyclopropanecarboxamido)pyridin-4-yl)benzamide Enantiomer 1 (25) and Enantiomer 2 (26). A 10 mL round-bottom flask was charged with *N*-(2-aminopyridin-4-yl)-2,6-dichlorobenzamide (28 mg, 0.10 mmol), followed by anhydrous DMF (1 mL), *trans*-2-fluorocyclopropanecarboxylic acid⁵⁴ (31 mg, 0.30 mmol), DIPEA (52 mg, 0.40 mmol), and HATU (114 mg, 0.30 mmol). The reaction mixture was stirred at room temperature under nitrogen for 18 h. The reaction mixture was diluted with a saturated NH₄Cl solution (20 mL) and extracted with EtOAc (2 × 20 mL). The combined organics were dried over Na₂SO₄, filtered, and concentrated via rotavap. The crude product was purified by chiral SFC (Chiralpak IC, 20% MeOH + 0.1% NEt₃, 5 min) to give two desired products as the following:

25: first eluting peak, 3.4 mg (9.2% yield), >99% ee (retention time 0.65 min, Chiralpak IC, 20% MeOH + 0.1% NEt₃, 5 min). ¹H NMR (400 MHz, DMSO-*d*₆): δ 11.14 (s, 1H), 10.88 (s, 1H), 8.38 (d, *J* = 1.6 Hz, 1H), 8.24 (d, *J* = 5.6 Hz, 1H), 7.62–7.55 (m, 2H), 7.51 (dd, *J* = 9.2, 6.8 Hz, 1H), 7.46 (dd, *J* = 5.6, 1.9 Hz, 1H), 4.86 (dddd, *J* = 64.7, 5.8, 3.2, 1.4 Hz, 1H), 2.56 (dddd, *J* = 22.3, 10.1, 6.4, 1.4 Hz, 1H), 1.51 (dddd, *J* = 22.3, 10.1, 6.4, 3.2 Hz, 1H), 1.23 (dddd, *J* = 12.9, 6.5, 6.4, 6.3 Hz, 1H). LCMS (ESI) *m/z*: 368.0 [M + H]⁺.

26: second eluting peak, 3.3 mg (9.0% yield), >99% ee (retention time 0.74 min, Chiralpak IC, 20% MeOH + 0.1% NEt₃, 5 min). ¹H NMR and LCMS match 25.

(1*R*,2*S*)-2-(4-(2,6-Dichlorobenzamido)pyridin-2-ylcarbamoyl)cyclopropanecarboxylic Acid (32). *Step 1.* A solution of *N*-(2-aminopyridin-4-yl)-2,6-dichlorobenzamide (1.41 g, 5 mmol) and 3-oxabicyclo[3.1.0]hexane-2,4-dione (2.24 g, 20 mmol) in 1,4-dioxane (25 mL) was heated at 90 °C under nitrogen for 4 h. The reaction mixture was cooled to room temperature and the precipitated white solid was collected by filtration to give 2,6-dichloro-*N*-(2-(2,4-dioxo-3-azabicyclo[3.1.0]hexan-3-yl)pyridin-4-yl)benzamide (1.28 g, 68% yield). ¹H NMR (400 MHz, DMSO-*d*₆): δ 11.42 (s, 1H), 8.47 (d, *J* = 5.6 Hz, 1H), 7.69 (d, *J* = 1.8 Hz, 1H), 7.67–7.59 (m, 3H), 7.55 (dd, *J* = 9.2, 6.8 Hz, 1H), 2.74 (dd, *J* = 8.0, 3.6 Hz, 2H), 1.69 (ddt, *J* = 20.6, 8.1, 4.2 Hz, 2H). LCMS (ESI) *m/z*: 376.0 [M + H]⁺.

Step 2. To a suspension of 2,6-dichloro-*N*-(2-(2,4-dioxo-3-azabicyclo[3.1.0]hexan-3-yl)pyridin-4-yl)benzamide (136 mg, 0.36 mmol) in THF (4.0 mL) was added a solution of LiOH (1 N, 2 mL, 2 mmol). The reaction mixture was stirred at room temperature for 2 h. The mixture was then extracted with EtOAc (10 mL). The aqueous layer was acidified with 1 N HCl to pH 2.0. The precipitated white solid was collected by filtration. The crude product was subsequently purified by chiral SFC (Chiralpak AD-H, 35% EtOH + 0.1% NEt₃, 6 min) to give two pure enantiomers as the following:

32: second eluting peak, 41 mg (29% yield), >99% ee (retention time 0.66 min, Chiralpak AD-H, 35% EtOH + 0.1% NEt₃, 3 min). ¹H NMR (400 MHz, DMSO-*d*₆): δ 12.10 (s, 1H), 11.13 (s, 1H), 10.85 (s, 1H), 8.36 (d, *J* = 1.5 Hz, 1H), 8.22 (d, *J* = 5.6 Hz, 1H), 7.61–7.55 (m, 2H), 7.54–7.50 (m, 1H), 7.48 (dd, *J* = 5.5, 1.8 Hz, 1H), 2.27 (dd, *J* = 14.6, 7.5 Hz, 1H), 2.01 (dd, *J* = 15.9, 8.5 Hz, 1H), 1.39 (td, *J* = 6.6, 4.2 Hz, 1H), 1.16 (td, *J* = 8.3, 4.1 Hz, 1H). LCMS (ESI) *m/z*: 394.0 [M + H]⁺.

Enantiomer of 32: first eluting peak, 43 mg (30% yield), >99% ee (retention time 0.56 min, Chiralpak AD-H, 35% EtOH + 0.1% NEt₃, 3 min). ¹H NMR and LCMS match 32.

2,6-Dichloro-4-cyano-*N*-(2-((1*R*,2*R*)-2-fluorocyclopropanecarboxamido)pyridin-4-yl)benzamide (35). *Step 1.* A solution of 2,6-dichloro-4-cyanobenzoic acid (324 mg, 1.5 mmol) in thionyl chloride (10 mL) was heated to reflux under nitrogen overnight. The next day, the reaction mixture was cooled to room temperature and volatiles were removed via rotavap. The corresponding acid chloride was obtained in quantitative yield as a yellow solid, which was used in the next step without purification.

Step 2. A 50 mL round-bottom flask was charged with 2-bromo-4-aminopyridine (295 mg, 1.5 mmol), followed by anhydrous DMF (5.0 mL). The resulting solution was cooled to 0 °C, and NaH (120 mg, 3.0 mmol, 60% dispersion in mineral oil) was added carefully under nitrogen. Ice bath was removed, and the mixture was warmed to room

temperature and stirred for 30 min before being cooled to 0 °C again. To this reaction mixture was slowly added a solution of the above acid chloride dissolved in anhydrous DMF (5.0 mL). The resulting mixture was stirred for another 1 h at room temperature. Then ice–water (20 mL) was added and the resulting mixture was extracted with ethyl acetate (3 × 50 mL). The combined organic layers were washed with brine (20 mL), dried over MgSO₄, and filtered. After removal of solvent under vacuum, the residue was purified by flash chromatography (ethyl acetate/petroleum ether = 1:10) to give *N*-(2-bromopyridin-4-yl)-2,6-dichloro-4-cyanobenzamide (389 mg, 70% yield). LCMS (ESI) *m/z*: 369.9 [M + H]⁺.

Step 3. To a 25 mL microwave tube was added *cis*-2-fluorocyclopropanecarboxamide (0.045 g, 0.44 mmol), followed by *N*-(2-bromopyridin-4-yl)-2,6-dichloro-4-cyanobenzamide (0.16 g, 0.40 mmol), Pd₂(dba)₃ (0.045 g, 0.049 mmol), XantPhos (0.035 g, 0.061 mmol), Cs₂CO₃ (0.51 g, 1.6 mmol), and 1,4-dioxane (6.0 mL). The mixture was degassed with nitrogen for 10 min. The tube was sealed and irradiated in a microwave reactor at 140 °C for 1 h before being cooled to room temperature. The mixture was filtered with Celite, and the filter cake was washed with additional EtOAc (2 × 10 mL). Combined filtrate was concentrated via rotavap, and the crude mixture was purified by preparative HPLC (Gilson GX 281; column, Shim-pack PRC-ODS 250 mm × 20 mm 15 μm; mobile phase CH₃CN/10 mM NH₄HCO₃; flow rate of 30 mL/min; run time of 17 min) to give the racemic mixture as a white solid (40 mg). This racemic mixture was then purified by chiral SFC (Chiralpak IC, 15% MeOH, 5 min) to give two pure enantiomers as following:

35: second eluting peak, 10 mg (6.4% yield), >99% ee (retention time 1.31 min, Chiralpak IC, 15% MeOH, 5 min). ¹H NMR (400 MHz, DMSO-*d*₆): δ 11.32 (s, 1H), 10.86 (s, 1H), 8.37 (d, *J* = 1.7 Hz, 1H), 8.32–8.24 (m, 3H), 7.49 (dd, *J* = 5.6, 1.9, 2.5 Hz, 1H), 4.95 (dddd, *J* = 66.2, 6.2, 6.2, 3.7 Hz, 1H), 2.21 (dddd, *J* = 9.1, 6.7, 6.2, 3.7 Hz, 1H), 1.63 (dddd, *J* = 23.2, 6.7, 6.2, 3.7 Hz, 1H), 1.16 (dddd, *J* = 12.4, 9.1, 6.2, 6.2 Hz, 1H). LCMS (ESI) *m/z*: 393.0 [M + H]⁺.

The other enantiomer was also obtained (12.5 mg, 8.0% yield), >99% ee (retention time 1.12 min, Chiralpak IC, 15% MeOH, 5 min). ¹H NMR and LCMS match **35**.

2-Chloro-4-cyano-6-fluoro-*N*-(2-((1*R*,2*R*)-2-fluorocyclopropanecarboxamido)pyridin-4-yl)benzamide (37). **Step 1.** A 10 mL round-bottom flask containing a suspension of 2-chloro-4-cyano-6-fluorobenzoic acid (443 mg, 2.22 mmol) in thionyl chloride (2.0 mL) was heated to reflux for 3 h under nitrogen. The mixture was cooled to room temperature, concentrated to dryness, and azeotroped with anhydrous toluene (2 × 5 mL) to give crude 2-chloro-4-cyano-6-fluorobenzoyl chloride as a white solid which was used in the next step without purification.

Step 2. A 25 mL round-bottom flask was charged with 4-amino-2-bromopyridine (346 mg, 2.0 mmol) and DIPEA (461 mg, 4.0 mmol), followed by anhydrous DCM (5.0 mL) and CH₃CN (0.5 mL). The resulting clear solution was cooled to 0 °C under nitrogen, and a solution of 2-chloro-4-cyano-6-fluorobenzoyl chloride (484 mg, 2.2 mmol) in DCM (2.0 mL) was added dropwise. Ice bath was removed, and the reaction mixture was warmed to room temperature and stirred for 16 h. The reaction mixture was diluted with a saturated NH₄Cl solution (40 mL) and extracted with EtOAc (3 × 50 mL). The combined organics were dried over Na₂SO₄, filtered, and concentrated to dryness. The crude product was purified by flash column chromatography on silica gel (0–50% EtOAc/hexane) to give *N*-(2-bromopyridin-4-yl)-2-chloro-4-cyano-6-fluorobenzamide as an off-white solid (379 mg, 53% yield).

Step 3. To a 25 mL microwave tube was added *N*-(2-bromopyridin-4-yl)-2-chloro-4-cyano-6-fluorobenzamide (681 mg, 1.92 mmol), followed by *cis*-2-fluorocyclopropanecarboxamide (218 mg, 2.11 mmol), Pd₂(dba)₃ (88 mg, 0.096 mmol), XantPhos (0.111 g, 192 mmol), Cs₂CO₃ (1.25 g, 3.84 mmol), 1,4-dioxane (10.0 mL), and 1,2-dimethoxyethane (3.0 mL). The mixture was degassed with nitrogen for 10 min. The tube was sealed and irradiated in a microwave reactor at 130 °C for 0.5 h. After being cooled to room temperature, the mixture was filtered with Celite and the filtrate was concentrated under vacuum. The resulting residue was purified by chiral SFC (Chiralpak

AS-H, 15% MeOH, 12 min) to give two pure enantiomers as the following:

37: second eluting peak, 288 mg (40% yield), >99% ee (retention time 1.23 min, Chiralpak AS-H, 15% MeOH, 2.5 min). ¹H NMR (400 MHz, DMSO-*d*₆): δ 11.33 (s, 1H), 10.82 (s, 1H), 8.35 (d, *J* = 1.6 Hz, 1H), 8.26 (d, *J* = 5.6 Hz, 1H), 8.17–8.08 (m, 2H), 7.49 (dd, *J* = 5.6, 1.9 Hz, 1H), 4.94 (dddd, *J* = 66.2, 6.3, 6.2, 3.7 Hz, 1H), 2.21 (dddd, *J* = 12.4, 9.2, 6.9, 6.3 Hz, 1H), 1.64 (dddd, *J* = 23.2, 6.9, 6.8, 3.7 Hz, 1H), 1.16 (dddd, *J* = 12.4, 9.2, 6.3, 6.3 Hz, 1H). LCMS (ESI) *m/z*: 377.1 [M + H]⁺.

The other enantiomer was also obtained (290 mg, 40% yield), >99% ee (retention time 1.03 min, Chiralpak AS-H, 15% MeOH, 2.5 min). ¹H NMR and LCMS data match **37**.

Computational Chemistry. To orthogonally validate the multipolar interaction described in ref 47 and depicted by Proasis for the TYK2 X-ray structures with **19** (Figure 3) and **35** (Figure 5), quantum calculations were carried out on model systems. The carbonyl was represented by a propan-2-one molecule, and the nitrile was represented by an acetonitrile molecule, both starting in the same coordinates as in the crystal structure of **19**. The program Jaguar (Schrodinger, Inc.) was used to carry out geometry optimization runs at the B3LYP/6-31G** level with PBF aqueous solvation for the propan-2-one alone, the acetonitrile alone, and the propan-2-one/acetonitrile complex with distance and angle constraints between the carbonyl and the nitrile to maintain the starting geometry of the complex. At the end of the geometry optimization runs, the interaction energy was calculated via subtraction of the sum of the solution phase energies for each separate molecule from the solution phase energy of the complex system. A similar method was used by Pierce and coworkers⁵⁵ to predict CH...O hydrogen bond strengths. Our calculation yielded an interaction energy of −0.9 kcal/mol, indicating a favorable interaction. To further verify the method and compare results with SAR, we used the same method on a system in which the acetonitrile was switched to a prop-1-yne. This system mimics compound **20**, and the resulting interaction energy was −0.1 kcal/mol, too small to conclude whether the interaction is favorable. This set of results is consistent with compound **19** having TYK2 *K*_i of 1.8 nM and compound **20** having TYK2 *K*_i of 9.5 nM.

■ ASSOCIATED CONTENT

● Supporting Information

Detailed experimental procedures for different benzoic acids and the rest of compounds shown in this work; single X-ray crystal structures of compounds **23** and **32**; crystallographic methods and procedures for **19** in complex with TYK2, **23** in complex with TYK2, and **35** in complex with TYK2; time course of mouse IL-12 PK/PD experiment. This material is available free of charge via the Internet at <http://pubs.acs.org>.

Accession Codes

PDB codes: 4GI1 for **19** complexed with TYK2, 4GJ2 for **23** complexed with TYK2, and 4GJ3 for **35** complexed with TYK2.

■ AUTHOR INFORMATION

Corresponding Author

*Phone: 650-467-3567, E-mail: liang.jun@gene.com.

Present Addresses

● A.v.A: Department of Cell Biology, Novartis, Emeryville, California.

△ W.B: Department of Infectious Disease, MedImmune, Gaithersburg, Maryland.

▽ J.D.: Department of Pharmacokinetics, Theravance, South San Francisco, California.

Notes

The authors declare no competing financial interest.

ACKNOWLEDGMENTS

We thank, Mengling Wong, Chris Hamman, Michael Hayes, Baiwei Lin, Deven Wang, Yutao Jiang for purification and analytical support; Daniel Hascall, Grady Howes, Gigi Yuen, and Garima Porwal for compound management support; Hoa Le and Qin Yue for ADME support; Emile Plise and Jonathan Cheng for MDCK data; Ning Liu for microsomal stability; Jasleen Sodhi for reversible CYP inhibition measurement; Quynh Ho for plasma protein binding measurement; Pete Dragovich, Steve Staben, and Kirk Robarge for many helpful comments and suggestions. Diffraction data were collected at the Stanford Synchrotron Radiation Lightsource, operated for the U.S. Department of Energy Office of Science by Stanford University, CA. The SSRL Structural Molecular Biology Program is supported by the DOE Office of Biological and Environmental Research, National Institute of General Medical Sciences (NIH) (including Grant P41GM103393), and the National Center for Research Resources (Grant P41RR001209).

ABBREVIATIONS USED

AIBN, 2,2'-azobis(2-methylpropionitrile); Arg, arginine; ATP, adenosine triphosphate; AUC, area under the curve; Boc₂O, di-*tert*-butyl dicarbonate; Boc, *tert*-butyl carbamate; brine, a saturated aqueous solution of sodium chloride; CHCl₃, chloroform; CH₃CN, acetonitrile; CL, clearance; C_{max}, maximum concentration; CCl₄, carbon tetrachloride; CL_p, clearance; Cs₂CO₃, cesium carbonate; CO, carbon monoxide; DavePhos, 2-dicyclohexylphosphino-2'-(*N,N*-dimethylamino)-biphenyl; DIPEA, *N,N*-diisopropylethylamine; DCM, dichloromethane; DMF, *N,N*-dimethylformamide; dppp, 1,3-bis-(diphenylphosphino)propane; EC₅₀, half maximal effective concentration; EPO, erythropoietin; EtOAc, ethyl acetate; EtOH, ethanol; Ex, example; *F*, oral bioavailability; Gln, glutamine; Glu, glutamic acid; HATU, *O*-(7-azabenzotriazol-1-yl)-*N,N,N',N'*-tetramethyluronium hexafluorophosphate; h, hour; H, hydrogen; HCl, hydrochloric acid; H₂O, water; HPLC, high performance liquid chromatography; H₂SO₄, sulfuric acid; *i*-BuNO₂, isobutyl nitrite; IBX, 2-iodoxybenzoic acid; IL-6, interleukin-6; IL-12, interleukin-12; IL-23, interleukin-23; IFN γ , interferon- γ ; iv, intravenous; ip, intraperitoneal; IPA, isopropyl alcohol; JAK, Janus kinase; biochemical JAK1 index, (JAK1 K_i)/(TYK2 K_i); cellular JAK1 index, (IL-6 pSTAT3 EC₅₀)/(IL-12 pSTAT4 EC₅₀); biochemical JAK2 index, (JAK2 K_i)/(TYK2 K_i); cellular JAK2 index, (EPO pSTAT5 EC₅₀)/(IL-12 pSTAT4 EC₅₀); K₂CO₃, potassium carbonate; K_i, inhibition constant; LCMS, liquid chromatography–mass spectrometry; LHDMS, lithium hexamethylidisilazide; LiI, lithium iodide; log *D*, log of partition coefficient between octanol and aqueous buffer; Leu, leucine; LM, liver microsome; MCT, methylcellulose/Tween; MDCK, Madin–Darby canine kidney; MeOH, methanol; min, minute; NaH, sodium hydride; NaHCO₃, sodium bicarbonate; NaNO₂, sodium nitrite; NCS, *N*-chlorosuccinimide; NEt₃, triethylamine; P_{app}, apparent permeability; Pd₂(dba)₃, tris-(dibenzylideneacetone)dipalladium; Pd(dppf)Cl₂, 1,1'-bis-(diphenylphosphino)ferrocenepalladium(II) dichloride; PK, pharmacokinetics; PK/PD, pharmacokinetics/pharmacodynamics; po, by mouth; PPB, plasma protein binding; SFC, supercritical fluid chromatography; STAT, signal transducer and activator of transcription; t_{1/2}, half-life; TFA, trifluoroacetic acid; Tf₂O, trifluoromethanesulfonic anhydride; THF, tetrahy-

drofuran; TLC, thin layer chromatography; tPSA, topological polar surface area; UV, ultraviolet; V_d, volume of distribution; XantPhos, 4,5-bis(diphenylphosphino)-9,9-dimethylxanthene

REFERENCES

- (a) Christophers, E. Psoriasis-epidemiology and clinical spectrum. *Clin. Exp. Dermatol.* **2001**, *26*, 314–320. (b) Lowes, M. A.; Bowcock, A. M.; Krueger, J. G. Pathogenesis and therapy of psoriasis. *Nature* **2007**, *445*, 866–873.
- (a) Abraham, C.; Cho, J. H. *N. Engl. J. Med.* **2009**, *361*, 2066–2078. (b) Garrette, W. S.; Gordon, J. L.; Glimcher, L. H. Homeostasis and inflammation in the intestine. *Cell* **2010**, *140*, 859–870. (c) Kaser, A.; Zeissig, S.; Blumberg, R. S. Inflammatory bowel disease. *Annu. Rev. Immunol.* **2010**, *28*, 573–621.
- (a) Gelfand, J. M.; Weinstein, R.; Porter, S. B.; Neimann, A. L.; Berlin, J. A.; Margolis, D. J. Prevalence and treatment of psoriasis in the United Kingdom—a population study. *Arch. Dermatol.* **2005**, *141*, 1537–1541. (b) Kurd, S. K.; Gelfand, J. M. The prevalence of previously diagnosed and undiagnosed psoriasis in US adults: results from NHANES 2003–2004. *J. Am. Acad. Dermatol.* **2009**, *60*, 218–224.
- (a) Mikhail, M.; Scheinfeld, N. S. Therapy treatment options for psoriasis: topical and systemic. *Therapy* **2004**, *1*, 319–330. (b) Nograles, K. E.; Krueger, J. G. Anti-cytokine therapies for psoriasis. *Exp. Cell Res.* **2011**, *317*, 1293–1300.
- Loftus, E. V. Clinical epidemiology of inflammatory bowel disease: incidence, prevalence, and environmental influences. *Gastroenterology* **2004**, *126*, 1504–1517.
- (a) Hanauer, S. B.; Feagan, B. G.; Lichtenstein, G. R.; Mayer, L. F.; Schreiber, S.; Colombel, J. F.; Rachmilewitz, D.; Wolf, D. C.; Olson, A.; Bao, W.; Rutgeerts, P. Maintenance infliximab for Crohn's disease: the ACCENT I randomized trial. *Lancet* **2002**, *359*, 1541–1549. (b) Rutgeerts, P.; Sandborn, W. J.; Feagan, B. G.; Reinisch, W.; Olson, A.; Johanns, J.; Travers, S.; Rachmilewitz, D.; Hanauer, S. B.; Lichtenstein, G.; de Villiers, W. J. S.; Present, D.; Sands, B. E.; Colombel, J. F. Infliximab for induction and maintenance therapy for ulcerative colitis. *N. Engl. J. Med.* **2005**, *353*, 2462–2476. (c) Ngo, B.; Farrell, C. P.; Barr, M.; Wolvo, K.; Bailey, R.; Mullin, J. M.; Thornton, J. J. Tumor necrosis factor blockade for treatment of inflammatory bowel disease: efficacy and safety. *Curr. Mol. Pharmacol.* **2010**, *3*, 145–152. (d) Caprioli, F.; Pallone, F.; Monteleone, G. Cytokine therapies in Crohn's disease: Where are we now and where should we go? *Inflammation Allergy* **2011**, *10*, 47–53.
- (a) Baer, F.; Noman, M.; Vermeire, S.; Assche, G. V.; Haens, G. D.; Cabonez, A.; Rutgeerts, P. Influence of immunogenicity on the long-term efficacy of infliximab in Crohn's disease. *N. Engl. J. Med.* **2003**, *348*, 601–608. (b) Ben-Horin, S.; Chowers, Y. Loss of response to anti-TNF treatments in Crohn's disease. *Aliment. Pharmacol. Ther.* **2011**, *33*, 987–995.
- (a) Bernstein, C. N.; Wajda, A.; Blanchard, J. F. The clustering of other chronic inflammatory disease in inflammatory bowel disease: a population-based study. *Gastroenterology* **2005**, *129*, 827–836. (b) de Mesquita, M. B.; Ferrante, M.; Henckaerts, L.; Joossens, M.; Jaessens, V.; Hlavaty, T.; Pierik, M.; Joossens, S.; Schuerbeek, M. V.; Assche, G. V.; Rutgeerts, P.; Vermeire, S.; Hoffman, I. Clustering of (auto)-immune diseases with early-onset and complicated inflammatory bowel disease. *Eur. J. Pediatr.* **2009**, *168*, 575–583. (c) Ellinghaus, D.; Ellinghaus, E.; Nair, R. P.; Stuart, P. E.; Esko, T.; Metspalu, A.; Debrus, S.; Raelson, J. V.; Tejasvi, T.; Belouchi, M.; West, S. L.; Barker, J. N.; Koks, S.; Kingo, K.; Balschun, T.; Palmieri, O.; Annesse, V.; Gieger, C.; Wichmann, H. E.; Kabesch, M.; Trembath, R. C.; Mathew, C. G.; Abecasis, G. R.; Weidinger, S.; Nikolaus, S.; Schreiber, S.; Elder, J. T.; Weichenthal, M.; Nothnagel, M.; Franke, A. Combined analysis of genome-wide association studies for Crohn's disease and psoriasis identifies seven shared susceptibility loci. *Am. J. Hum. Genet.* **2012**, *90*, 636–645. (d) Lees, C. W.; Barrett, J. C.; Parkes, M.; Satsangi, J. New IBD genetics: common pathways with other diseases. *Gut* **2011**, *60*, 1739–1753.

(9) (a) Sweeney, C.; Tobin, A.-M.; Kirby, B. Innate immunity in the pathogenesis of psoriasis. *Arch. Dermatol. Res* **2011**, *303*, 691–705. (b) Monteleone, G.; Pallone, F.; MacDonald, T. Emerging immunological targets in inflammatory bowel disease. *Curr. Opin. Pharmacol.* **2011**, *11*, 640–645.

(10) (a) Mucida, D.; Cheroutre, H. The many face-lifts of CD4 T helper cells. *Adv. Immunol.* **2010**, *107*, 139–152. (b) O'Garra, A.; Robinson, D. Development and function of T-helper 1 cells. *Adv. Immunol.* **2004**, *83*, 133–162. (c) Murphy, K. M.; Reiner, S. The lineage decisions of helper T cells. *Nat. Rev. Immunol.* **2002**, *2*, 933–944.

(11) (a) Skokos, D.; Waite, J. C. Th17 response and inflammatory autoimmune diseases. *Int. J. Inflammation* **2012**, 819467. (b) Miossec, P.; Korn, T.; Kuchroo, V. K. Interleukin-17 and type 17 helper cells. *N. Engl. J. Med.* **2009**, *361*, 888–898. (c) Louten, J.; Boniface, K.; Malefyt, R. d. W. Development and function of Th17 cells in health and disease. *J. Allergy Clin. Immunol.* **2009**, *123*, 1004–1011. (d) Boniface, K.; Blom, B.; Liu, Y.-J.; Malefyt, R. d. W. From interleukin-23 to T-helper 17 cells: human T-helper cell differentiation revisited. *Immunol. Rev.* **2008**, *226*, 132–146.

(12) (a) Trinchieri, G. Interleukin-12: a proinflammatory cytokine with immunoregulatory functions that bridge innate resistance and antigen-specific adaptive immunity. *Annu. Rev. Immunol.* **1995**, *13*, 251–276. (b) Chung, Y.; Dong, C. Don't leave home without it: the IL-23 visa to Th17 cells. *Nat. Immunol.* **2009**, *10*, 236–238.

(13) (a) Chua, A. O.; Chizzonite, R.; Desai, B. B.; Truitt, T. P.; Nunes, P.; Minetti, L. J.; Warrior, R. R.; Presky, D. H.; Levine, J. F.; Gately, M. K.; Gubler, U. Expression cloning of a human IL-12 receptor component. *J. Immunol.* **1994**, *153*, 128–136. (b) Presky, D. H.; Yang, H.; Minetti, L. J.; Chua, A. O.; Nabavi, N.; Wu, C.-Y.; Gately, M. K.; Gubler, U. A functional interleukin 12 receptor complex is composed of two β -type cytokine receptor subunits. *Proc. Natl. Acad. Sci. U.S.A.* **1996**, *93*, 14002–14007.

(14) Parham, C.; Chirica, M.; Timans, J.; Vaisberg, E.; Travis, M.; Cheung, J.; Pflanz, S.; Zhang, R.; Singh, K.; Vega, F.; To, W.; Wagner, J.; O'Farrell, A.-M.; McClanahan, T.; Zurawski, S.; Hannum, C.; Gorman, D.; Rennick, D.; Kastlein, R. A.; Malefyt, R. d. W.; Moore, K. W. A receptor for the heterodimeric cytokine IL-23 is composed of IL-12 β 1 and a novel cytokine receptor subunit, IL-23R. *J. Immunol.* **2002**, *168*, 5699–5708.

(15) (a) Firmbach-Kraft, I.; Byers, M.; Shows, T.; Dalla-Favera, R.; Krolewski, J. J. TYK2, prototype of a novel class of non-receptor tyrosine kinase genes. *Oncogene* **1990**, *5*, 1329–1336. (b) Zou, J.; Presky, D. H.; Wu, C.-Y.; Gubler, U. Differential associations between the cytoplasmic regions of the interleukin-12 receptor subunits β 1 and β 2 and JAK kinases. *J. Biol. Chem.* **1997**, *272*, 6073–6077.

(16) (a) Harpur, A. G.; Andres, A. C.; Ziemiecki, A.; Aston, R. R.; Wilks, A. F. JAK2, a third member of the JAK family of protein tyrosine kinases. *Oncogene* **1992**, *7*, 1347–1353. (b) Yamamoto, K.; Shibata, F.; Miura, O.; Kamiyama, R.; Hirosawa, S.; Miyasaka, N. Physical interaction between interleukin-12 receptor β 2 subunit and JAK2 tyrosine kinase: JAK2 associates with cytoplasmic membrane-proximal region of interleukin-12 receptor β 2 via amino terminus. *Biochem. Biophys. Res. Commun.* **1999**, *257*, 400–404.

(17) Wilks, A. F.; Harpur, A. G.; Kurban, R. R.; Ralph, S. J.; Zurcher, G.; Ziemiecki, A. Two novel protein-tyrosine kinases, each with a second phosphotransferase-related catalytic domain, define a new class of protein kinase. *Mol. Cell. Biol.* **1991**, *11*, 2057–2065.

(18) (a) Rane, S. G.; Reddy, P. E. JAK3: a novel JAK kinase associated with terminal differentiation of hematopoietic cells. *Oncogene* **1994**, *9*, 2045–2052. (b) Takahashi, T.; Shirasawa, T. Molecular cloning of rat JAK3, a novel member of the JAK family of protein tyrosine kinases. *FEBS Lett.* **1994**, *342*, 124–128.

(19) (a) Shaker, O. G.; Moustafa, W.; Essmat, S.; Abdel-Halim, M.; El-Komy, M. The role of interleukin-12 in the pathogenesis of psoriasis. *Clin. Biochem.* **2006**, *39*, 119–125. (b) Piskin, G.; Sylva-Steenland, R. M. R.; Bos, J. D.; Teunissen, M. B. M. In vitro and in situ expression of IL-23 by keratinocytes in healthy skin and psoriasis lesions: enhanced expression in psoriatic skin. *J. Immunol.* **2006**, *176*,

1908–1915. (c) Lee, E.; Trepicchio, W. L.; Oestreicher, J.; Pittman, D.; Wang, F.; Chamian, F.; Dhodapkar, M.; Krueger, J. G. Increased expression of interleukin 23p19 and p40 in lesional skin of patients with psoriasis vulgaris. *J. Exp. Med.* **2004**, *199*, 125–130. (d) Yawalkar, N.; Karlen, S.; Hunger, R.; Brand, C. U.; Braathen, L. R. Expression of interleukin-12 is increased in psoriatic skin. *J. Invest. Dermatol.* **1998**, *111*, 1053–1057.

(20) (a) Tada, Y.; Asahina, A.; Takekoshi, T.; Kishimoto, E.; Mitsui, H.; Saeki, H.; Komine, M.; Tamaki, K. Interleukin 12 production by monocytes from patients with psoriasis and its inhibition by cyclosporin A. *Br. J. Dermatol.* **2006**, *154*, 1180–1183. (b) Chamian, F.; Lowes, M. A.; Lin, S.-L.; Lee, E.; Kikuchi, T.; Gilleaudeau, P.; Sullivan-Whalen, M.; Cardinale, I.; Khatcherian, A.; Novitskaya, I.; Wittkowski, K. M.; Krueger, J. G. Alefacept reduces infiltrating T cells, activated dendritic cells, and inflammatory genes in psoriasis vulgaris. *Proc. Natl. Acad. Sci. U.S.A.* **2005**, *102*, 2075–2080. (c) Gottlieb, A. B.; Chamian, F.; Masud, S.; Cardinale, I.; Abello, M. V.; Lowes, M. A.; Chen, F.; Magliocco, M.; Krueger, J. G. TNF inhibition rapidly down-regulates multiple proinflammatory pathways in psoriasis plaques. *J. Immunol.* **2005**, *175*, 2721–2729. (d) Piskin, G.; Tursen, U.; Sylva-Steenland, R. M.; Bos, J. D.; Teunissen, M. B. M. Clinical improvement in chronic plaque-type psoriasis lesions after narrow-band UVB therapy is accompanied by a decrease in the expression of IFN γ inducers—IL-12, IL-18 and IL-23. *Exp. Dermatol.* **2004**, *13*, 764–772.

(21) (a) Kopp, T.; Lenz, P.; Bello-Fernandez, C.; Kastelein, R.; Kupper, T. S.; Stingl, G. IL-23 production by co-secretion of endogenous p19 and transgenic p40 in keratin 14/p40 transgenic mice: evidence for enhanced cutaneous immunity. *J. Immunol.* **2003**, *170*, 5438–5444. (b) Kopp, T.; Kieffer, J. D.; Rot, A.; Strommer, S.; Stingl, G.; Kupper, T. S. Inflammatory skin disease in K14/p40 transgenic mice: evidence for interleukin-12-like activities of p40. *J. Invest. Dermatol.* **2001**, *117*, 618–626.

(22) Clarke, A. W.; Poulton, L.; Wai, H. Y.; Walker, S. A.; Victor, S. D.; Domagala, T.; Mraovic, D.; Butt, D.; Shewmaker, N.; Hennings, P.; Doyle, A. G. A novel class of anti-IL-12p40 antibodies. *mAbs* **2010**, *2*, 539–549.

(23) (a) Kimball, A. B.; Gordon, K. B.; Fakhrazadeh, S.; Yeilding, N.; Szapary, P. O.; Schenkel, B.; Guzzo, C.; Li, S.; Papp, K. A. Long-term efficacy of ustekinumab in moderate-to-severe psoriasis: results from the PHOENIX 1 trials through up to 3 years. *Br. J. Dermatol.* **2012**, *166*, 861–872. (b) Papp, K. A.; Langley, R. G.; Lebwohl, M.; Krueger, G. G.; Szapary, P.; Yeilding, N.; Guzzo, C.; Hsu, M.-C.; Wang, Y.; Li, S.; Dooley, L. T.; Reich, K. Efficacy and safety of ustekinumab, a human interleukin-12/23 monoclonal antibody, in patients with psoriasis: 52-week results from a randomized, double-blind, placebo-controlled trial (PHOENIX 2). *Lancet* **2008**, *371*, 1675–1684. (c) Leonardi, G. L.; Kimball, A. B.; Papp, K. A.; Yeilding, N.; Guzzo, C.; Wang, Y.; Li, S.; Dooley, L. T.; Gordon, K. B. Efficacy and safety of ustekinumab, a human interleukin-12/23 monoclonal antibody, in patients with psoriasis: 76-week results from a randomized, double-blind, placebo-controlled trial (PHOENIX 1). *Lancet* **2008**, *371*, 1665–1674.

(24) Benson, J. M.; Sachs, C. W.; Treacy, G.; Zhou, H.; Pendley, C.; Brodmerkel, C. M.; Shankar, G.; Mascelli, M. A. Therapeutic targeting of the IL-12/23 pathways: generation and characterization of ustekinumab. *Nat. Biotechnol.* **2011**, *29*, 615–624.

(25) (a) Barrett, J. C.; Hansoul, S.; Nicolae, D. L.; Cho, J. H.; Duerr, R. H.; Rioux, J. D.; Brant, S. R.; Silverberg, M. K.; Taylor, K. D.; Barmada, M. M.; Bitton, A.; Dassopoulos, T.; Datta, L. W.; Green, T.; Griffiths, A. M.; Kistner, E. O.; Murtha, M. T.; Regueiro, M. D.; Rotter, J. T.; Schumm, L. P.; Steinhart, A. H.; Targan, S. T.; Xavier, R. J.; Libioulle, C.; Sandor, C.; Lathrop, M.; Belaiche, J.; Dewit, O.; Gut, I.; Heath, S.; Laukens, D.; Mni, M.; Rutgeerts, P.; Gossom, A. v.; Zelenika, D.; Franchimont, D.; Hugot, J.-P.; de Vos, M.; Vermeire, S.; Louis, E.; Cardon, L. R.; Anderson, C. A.; Drummond, H.; Nimmo, E.; Ahmad, T.; Prescott, N. J.; Onnie, C. M.; Fisher, S. A.; Marchini, J.; Ghorji, J.; Bumpstead, S.; Gwilliam, R.; Tremelling, M.; Deloukas, P.; Mansfield, J.; Jewel, D.; Satsangi, J.; Mathew, C. G.; Parkes, M.; Georges, M.; Daly, M. J. Genome-wide association defines more than

30 distinct susceptibility loci for Crohn's disease. *Nat. Genet.* **2008**, *40*, 955–962. (b) Duerr, R. H.; Taylor, K. D.; Brant, S. R.; Rioux, J. D.; Silverberg, M. S.; Daly, M. J.; Steinhardt, A. H.; Abraham, C.; Regueiro, M.; Griffiths, A.; Dassopoulos, T.; Bitton, A.; Yang, H.; Targan, S.; Datta, L. W.; Kistner, E. O.; Schumm, L. P.; Lee, A. T.; Gregersen, P. K.; Barnada, M. M.; Rotter, J. I.; Nicolae, D. L.; Cho, J. H. A genome-wide association study identifies IL23R as an inflammatory bowel disease gene. *Science* **2006**, *314*, 1461–1463.

(26) (a) Hue, S.; Ahern, P.; Bounocore, S.; Kullberg, M. C.; Cua, D. J.; McKenzie, B. S.; Pwrie, F.; Maloy, K. J. Interleukin-23 drives innate and T cell-mediated intestinal inflammation. *J. Exp. Med.* **2006**, *203*, 2473–2483. (b) Kullberg, M. C.; Jankovic, D.; Feng, C. G.; Hue, S.; Gorelick, P. L.; McKenzie, B. S.; Cua, D. J.; Powrie, F.; Cheever, A. W.; Maloy, K. J.; Sher, A. IL-23 plays a key role in *Helicobacter hepaticus*-induced T cell-dependent colitis. *J. Exp. Med.* **2006**, *203*, 2485–2494.

(27) Sandborn, W. J.; Feagan, B.; Fedorak, R. N.; Scherl, E.; Fleisher, M. R.; Katz, S.; Johanns, J.; Blank, M.; Rutgeerts, P. A randomized trial of ustekinumab, a human interleukin-12/23 monoclonal antibody, in patients with moderate-to-severe Crohn's disease. *Gastroenterology* **2008**, *135*, 1130–1141.

(28) (a) Kralovics, R.; Passamonti, F.; Buser, A. S.; Teo, S.-S.; Tiedt, R.; Passweg, J. R.; Tichelli, A.; Cazzola, M.; Skoda, R. A gain-of-function mutation of JAK2 in myeloproliferative disorders. *N. Engl. J. Med.* **2005**, *352*, 1779–1790. (b) James, C.; Ugo, V.; Couedic, J.-P.; Staerk, J.; Delhommeau, F.; Lacout, C.; Garcon, L.; Raslova, H.; Berger, R.; Bennaceur-Griscelli, A.; Villeval, J. L.; Constantinescu, S. N.; Casadevall, N.; Vainchenker, W. A unique clonal JAK2 mutation leading to constitutive signaling causes polythemia vera. *Nature* **2005**, *434*, 1144–1148.

(29) (a) Parganas, E.; Wang, D.; Stravopodis, D.; Topham, D. J.; Marine, J. C.; Teglund, S.; Vanin, E. F.; Bodner, S.; Colamonici, O. R.; van Deursen, J. M.; Grosveld, G.; Ihle, J. N. JAK2 is essential for signaling through a variety of cytokine receptors. *Cell* **1998**, *93*, 385–395. (b) Neubauer, H.; Cumano, A.; Muller, M.; Wu, H.; Huffstadt, U.; Pfeffer, K. JAK2 deficiency defines an essential developmental checkpoint in definitive hematopoiesis. *Cell* **1998**, *93*, 397–409.

(30) (a) Tefferi, A. JAK inhibitors for myeloproliferative neoplasms: clarifying facts from myths. *Blood* **2012**, *119*, 2721–2730. (b) Pardanani, A.; Gotlib, J.; Jamieson, C.; Cortes, J. E.; Talpaz, M.; Stone, R. M.; Silverman, M. H.; Gilliland, D. G.; Shorr, J.; Tefferi, A. Safety and efficacy of TG101348, a selective JAK2 inhibitor, in myelofibrosis. *J. Clin. Oncol.* **2011**, *29*, 789–796. (c) Verstovsek, S.; Kantarjian, H.; Mesa, R. A.; Pardanani, A.; Cortes-Franco, J.; Thomas, D. A.; Estrov, Z.; Fridman, J. S.; Bradley, E. C.; Erickson-Viitanen, S.; Vaddi, K.; Levy, R.; Tefferi, A. Safety and efficacy of INCB018424, a JAK1 and JAK2 inhibitor, in myelofibrosis. *N. Eng. J. Med.* **2010**, *363*, 1117–1127.

(31) Ishizaki, M.; Akimoto, T.; Muromoto, R.; Yokoyama, M.; Ohshira, Y.; Sekine, Y.; Maeda, H.; Shimoda, K.; Oritani, K.; Matsuda, T. Involvement of tyrosine kinase-2 in both the IL-12/Th1 and IL-23/Th17 axes in vivo. *J. Immunol.* **2011**, *187*, 181–89.

(32) Minegishi, Y.; Saito, M.; Morio, T.; Watanabe, K.; Agematsu, K.; Tsuchiya, S.; Takada, H.; Hara, T.; Kawamura, N.; Ariga, T.; Kaneko, H.; Kondo, N.; Tsuge, I.; Yachie, A.; Sakiyama, Y.; Iwata, T.; Bessho, F.; Ohishi, T.; Joh, K.; Imai, K.; Kogawa, K.; Shinohara, M.; Fujieda, M.; Wakiguchi, H.; Pasic, S.; Abinun, M.; Ochs, H. D.; Renner, E. D.; Jansson, A.; Belohradsky, B. H.; Melin, A.; Shimizu, N.; Mizutani, S.; Miyawaki, T.; Nonoyama, S.; Karasuyama, H. Human tyrosine kinase 2 deficiency reveals its requisite roles in multiple cytokine signals involved in innate and acquired immunity. *Immunity* **2006**, *25*, 745–755.

(33) Sohn, S. J.; Barrett, K.; van Abbema, A.; Chang, C.; Kohli, P. B.; Kanda, H.; Smith, J.; Lai, Y.; Zhou, A.; Williams, K.; Macleod, C.; Hurley, C. A.; Kulagowski, J. K.; Lewis-Koh, N.; Johnson, A. R.; Ghilardi, N.; Zak, M.; Liang, J.; Blair, W. S.; Magnuson, S.; Wu, L. C. A restricted role for TYK2 catalytic activity in human cytokine response. *J. Immunol.*, submitted.

(34) (a) Tanaka, T.; Kishimoto, T. Immunotherapeutic implication of IL-6 blockade. *Immunotherapy* **2012**, *4*, 87–105. (b) Rodig, S. J.;

Meraz, M. A.; White, J. M.; Lampe, P. A.; Riley, J. K.; Arthur, C. A.; King, K. L.; Sheehan, K. C. F.; Yin, L.; Pennica, D.; Johnson, E. M.; Schreiber, R. D. Disruption of the JAK1 gene demonstrates obligatory and nonredundant roles of the JAKs in cytokine-induced biologic response. *Cell* **1998**, *93*, 373–383.

(35) (a) Comejo, M. G.; Boggon, T. J.; Mercher, T. JAK3: a two-faced player in hematological disorders. *Int. J. Biochem. Cell Biol.* **2009**, *41*, 2376–2379. (b) Pesu, M.; Candotti, F.; Husa, M.; Hofmann, S. R.; Notarangelo, L. D.; O'Shea, J. J. JAK3, severe combined immunodeficiency, and a new class of immunosuppressive drugs. *Immunol. Rev.* **2005**, *203*, 127–142.

(36) (a) Candotti, F.; Oakes, S. A.; Johnson, J. A.; Giliani, S.; Schumacher, R. F.; Mella, P.; Fioini, M.; Ugazio, A. G.; Badolato, R.; Notarangelo, L. D.; Bozzi, F.; Macchi, P.; Strina, D.; Vezzoni, P.; Blaese, R. M.; O'Shea, J. J.; Villa, A. Structural and functional basis for JAK3-deficient severe combined immunodeficiency. *Blood* **1997**, *90*, 3996–4003. (b) Russell, S. M.; Tayebi, N.; Nakajima, H.; Riedy, M. C.; Roberts, J.; Aman, M. J.; Migone, T.-S.; Noguchi, M.; Markert, M. L.; Buckley, R. H.; O'Shea, J. J.; Leonard, W. J. Mutation of JAK3 in a patient with SCID: essential role of JAK3 in lymphoid development. *Science* **1995**, *270*, 797–800.

(37) Flanagan, M. E.; Blumenkopf, T. A.; Brissette, W. H.; Brown, M. F.; Casavant, J. M.; Shang-Poa, C.; Doty, J. L.; Elliott, E. A.; Fisher, M. B.; Hines, M.; Kent, C.; Kudlacz, E. M.; Littie, B. M.; Magnusson, K. S.; McCurdy, S. P.; Munchhof, M. J.; Perry, B. D.; Sawyer, P. S.; Strelevitz, T. J.; Subramanyam, C.; Sun, J.; Whipple, D. A.; Changelian, P. S. Discovery of CP-690,550: a potent and selective Janus kinase (JAK) inhibitor for the treatment of autoimmune diseases and organ transplant rejection. *J. Med. Chem.* **2010**, *53*, 8468–8484.

(38) Quintas-Cardama, A.; Vaddi, K.; Liu, P.; Manshour, T.; Li, J.; Scherle, P. A.; Caulder, E.; Wen, X.; Li, Y.; Waeltz, P.; Rupar, M.; Burn, T.; Lo, Y.; Kelley, J.; Covington, M.; Shepard, S.; Rodgers, J. D.; Haley, P.; Kantarjian, H.; Fridman, J. S.; Verstovsek, S. Preclinical characterization of the selective JAK1/2 inhibitor INCB018424: therapeutic implications for the treatment of myeloproliferative neoplasms. *Blood* **2010**, *115*, 3109–3117.

(39) Alicea-Velazquez, N. L.; Boggon, T. J. The use of structural biology in Janus kinase targeted drug discovery. *Curr. Drug Targets* **2011**, *12*, 546–555.

(40) Goodacre, S. C.; Lai, Y.; Liang, J.; Magnuson, S. R.; Robarge, K. D.; Stanley, M. S.; Tsui, V.; Williams, K.; Zhang, B.; Zhou, A. Janus Kinase Inhibitor Compounds and Methods. WO2010142752, 2010. The following patent applications describing TYK2 inhibitors were also published: (a) Buchmann, B.; Eis, K.; Bothe, U.; Bonin, A.; Bomer, U.; Carbonylamino-Substituierte Aniline-Pyrimidin derivative als TYK-Inhibitoren, deren Herstellung und Verwendung als Arzneimittel. DE2009001438, 2009. (b) Boys, M. L.; Burgess, L. E.; Groneberg, R. D.; Harvey, D. M.; Huang, L.; Kercher, T.; Kraser, C. F.; Laird, E.; Tarlton, E.; Zhao, Q. 5,7-Substituted-imidazo[1,2-c]pyrimidines as Inhibitors of JAK Kinases. WO2011130146, 2011. (c) Ellard, K.; Major, J.; Jones, A.; Lynch, R.; Ramsden, N. Pyridine Compounds and Aza Analogs Thereof as TYK2 Inhibitors. WO2012062704, 2012.

(41) Liang, J.; Tsui, V.; van Abbema, A.; Bao, L.; Barrett, K.; Beresini, M.; Berezhkovsky, B.; Blair, W.; Chang, C.; Driscoll, J.; Eigenbrot, C.; Ghilardi, N.; Gibbons, P.; Halladay, J.; Johnson, A.; Kohli, P. B.; Lai, Y.; Liimatta, M.; Mantik, P.; Menghrajani, K.; Murray, J.; Sambrook, A.; Shao, Y.; Shia, S.; Shin, Y.; Smith, J.; Sohn, S.; Stanley, M.; Ultsch, M.; Zhang, B.; Magnuson, S. Lead identification of novel and selective TYK2 inhibitors. *Eur. J. Med. Chem.*, accepted.

(42) Our compounds were found to be consistently much less active against the JAK3 enzyme than TYK2 (>50-fold difference between the JAK3 K_i and TYK2 K_i). JAK3 inhibitory activities were not reported for the majority of compounds described in this work except for compound 3 (Figure 1) and compounds 35–37 (Table 3). Recent reports also suggested that JAK3 inhibition is not sufficient in blocking effects of type I cytokines and that JAK1 is the dominant kinase: (a) Haan, C.; Rovlering, C.; Rault, F.; Kapp, M.; Druckes, P.; Thoma, G.; Behrmann, I.; Zerwes, H.-G. JAK1 has a dominant role over JAK3

- in signal transduction through γ c-containing cytokine receptors. *Chem. Biol.* **2011**, *18*, 314–323. (b) Thoma, G.; Nuninger, F.; Falchetto, R.; Hermes, E.; Tavares, G. A.; Vangrevelinghe, E.; Zerwes, H.-G. Identification of a potent Janus kinase 3 inhibitor with high selectivity within the Janus kinase family. *J. Med. Chem.* **2011**, *54*, 284–288.
- (43) (a) Hughes, J. D.; Blagg, J.; Price, D. A.; Bailey, S.; DeCrescenzo, G. A.; Devraj, R. V.; Ellworth, E.; Fobian, Y. M.; Gibbs, M. E.; Gilles, R. W.; Greene, N.; Huang, E.; Krieger-Burke, T.; Loesel, J.; Wager, T.; Whiteley, L.; Zhang, Y. Physicochemical drug properties associated with in vivo toxicological outcomes. *Bioorg. Med. Chem. Lett.* **2008**, *18*, 4872–4875. (b) Leeson, P. D.; Spingthorpe, B. The influence of drug-like concepts on decision-making in medicinal chemistry. *Nat. Rev. Drug Discovery* **2007**, *6*, 881–890.
- (44) Kinase P-loop is known to be flexible: (a) Taylor, S. S.; Kornev, A. P. Protein kinases: evolution of dynamic regulatory protein. *Trends Biochem. Sci.* **2011**, *36*, 65–77. (b) Kornev, A. P.; Taylor, S. S. Defining the conserved internal architecture of a protein kinase. *Biochim. Biophys. Acta* **2010**, *1804*, 440–444.
- (45) Cruciani, G.; Carosati, E.; De Boeck, B.; Ethirajulu, K.; Mackie, C.; Howe, T.; Vianello, R. Metasite: understanding metabolism in human cytochromes from the perspective of the chemist. *J. Med. Chem.* **2005**, *48*, 6970–6979.
- (46) (a) Hill, A. P.; Young, R. J. Getting physical in drug discovery: a contemporary perspective on solubility and hydrophobicity. *Drug Discovery Today* **2010**, *15*, 648–655. (b) Richie, T. J.; MacDonald, S. J. F. The impact of aromatic ring count on compound developability—Are too many aromatic rings a liability in drug design? *Drug Discovery Today* **2009**, *14*, 1011–1020.
- (47) Paulini, R.; Müller, K.; Diederich, F. Orthogonal multipolar interactions in structural chemistry and biology. *Angew. Chem., Int. Ed.* **2005**, *44*, 1788–1805.
- (48) Kuhn, B.; Fuchs, J. E.; Reutlinger, M.; Stahl, M.; Taylor, N. R. Rationalizing tight ligand binding through cooperative interaction networks. *J. Chem. Inf. Model.* **2011**, *51*, 3180–3198.
- (49) (a) Tsui, V.; Gibbons, P.; Ultsch, M.; Mortara, K.; Chang, C.; Blair, W.; Pulk, R.; Stanley, M.; Starovasnik, M.; Williams, D.; Lamers, M.; Leonard, P.; Magnuson, S.; Liang, J.; Eigenbrot, C. A new regulatory switch in a JAK protein kinase. *Proteins: Struct., Funct., Bioinf.* **2011**, *79*, 393–401. (b) Chrencik, J. E.; Patny, A.; Leung, I. K.; Korniski, B.; Emmons, T. L.; Hall, T.; Weinberg, R. A.; Gormley, J. A.; Williams, J. M.; Day, J. E.; Hirsch, J. L.; Kiefer, J. R.; Leone, J. W.; Fischer, H. D.; Sommers, C. D.; Huang, H.-C.; Jacobsen, E. J.; Tenbrink, R. E.; Tomasselli, A. G.; Benson, T. E. Structural and thermodynamic characterization of the TYK2 and JAK3 kinase domains in complex with CP-690550 and CMP-6. *J. Mol. Biol.* **2010**, *400*, 413–433.
- (50) Knight, Z. A.; Shokat, K. M. Features of selective kinase inhibitors. *Chem. Biol.* **2005**, *12*, 621–637.
- (51) Graczyk, P. P. Gini coefficient: a new way to express selectivity of kinase inhibitors against a family of kinases. *J. Med. Chem.* **2007**, *50*, 5773–5779.
- (52) (a) Böhm, H.-J.; Banner, D.; Bendels, S.; Kansy, M.; Kuhn, B.; Müller, K.; Obst-Sander, U.; Stahl, M. Fluorine in medicinal chemistry. *ChemBioChem* **2004**, *5*, 637–643. (b) Purser, S.; Moore, P. R.; Swallow, S.; Gouverneur, V. Fluorine in medicinal chemistry. *Chem. Soc. Rev.* **2008**, *37*, 320–330. (c) Hagmann, W. K. The many roles for fluorine in medicinal chemistry. *J. Med. Chem.* **2008**, *51*, 4359–4369.
- (53) The relatively small shift (4.4-fold) of potency between PBMC and human whole blood for compound **37** is likely due to its modest (86.6%) human plasma protein binding (Table 4). A nice review of “free drug principle” with many recent examples could be found: Trainor, G. L. *Expert Opin. Drug Discovery* **2007**, *2*, 51–64.
- (54) Synthesis and chiral resolution of 2-fluorocyclopropanecarboxylic acid have been reported: (a) Akiba, T.; Ikeya, T.; Kawanishi, H.; Yukimoto, Y.; Kamihara, S.; Ebata, T. Selective Dehalogenation Process. U.S. Patent 5,780,669, 1998. (b) Kimura, Y.; Atarashi, S.; Kawakami, K.; Sato, K.; Hayakawa, I. (Fluorocyclopropyl)quinolones. 2. Synthesis and stereochemical structure–activity relationship of chiral 7-(7-amino-5-azaspiro[2.4]heptan-5-yl)-1-(2-fluorocyclopropyl)quinolone antibacterial agents. *J. Med. Chem.* **1994**, *37*, 3344–3352.
- (55) Pierce, A. C.; Sandretto, K. L.; Bemis, G. W. Kinase inhibitors and the case for CH...O hydrogen bonds in protein-ligand binding. *Proteins* **2002**, *49*, 567–576.